

A mathematical model of the mevalonate cholesterol biosynthesis pathway

Article

Accepted Version

Creative Commons: Attribution-Noncommercial-No Derivative Works 4.0

Pool, F., Currie, R., Sweby, P. K., Salazar, J. D. and Tindall, M. J. (2018) A mathematical model of the mevalonate cholesterol biosynthesis pathway. *Journal of Theoretical Biology*, 443. pp. 157-176. ISSN 0022-5193 doi: <https://doi.org/10.1016/j.jtbi.2017.12.023> Available at <http://centaur.reading.ac.uk/74972/>

It is advisable to refer to the publisher's version if you intend to cite from the work. See [Guidance on citing](#).

To link to this article DOI: <http://dx.doi.org/10.1016/j.jtbi.2017.12.023>

Publisher: Elsevier

All outputs in CentAUR are protected by Intellectual Property Rights law, including copyright law. Copyright and IPR is retained by the creators or other copyright holders. Terms and conditions for use of this material are defined in the [End User Agreement](#).

www.reading.ac.uk/centaur

CentAUR

Central Archive at the University of Reading

Reading's research outputs online

1 A mathematical model of the mevalonate cholesterol
2 biosynthesis pathway

3 Frances Pool^a, Richard Currie^b, Peter K. Sweby^c, José Domingo Salazar^d,
4 Marcus J. Tindall^{c,e,*}

5 ^a*Institute of Ophthalmology, University College London, Gower Street, London, United*
6 *Kingdom, WC1E 6BT.*

7 ^b*Syngenta, Jealott's Hill International Research Centre, Bracknell, Berkshire, United*
8 *Kingdom, RG42 6EY.*

9 ^c*Department of Mathematics and Statistics, University of Reading, Whiteknights,*
10 *Reading, United Kingdom, RG6 6AX.*

11 ^d*AstraZeneca, Unit 310, Cambridge Science Park, Milton Road, Cambridge,*
12 *Cambridgeshire, United Kingdom, CB4 0FZ*

13 ^e*Institute of Cardiovascular and Metabolic Research, University of Reading,*
14 *Whiteknights, Reading, United Kingdom, RG6 6AA.*

15 **Abstract**

We formulate, parameterise and analyse a mathematical model of the mevalonate pathway, a key pathway in the synthesis of cholesterol. Of high clinical importance, the pathway incorporates rate limiting enzymatic reactions with multiple negative feedbacks. In this work we investigate the pathway dynamics and demonstrate that rate limiting steps and negative feedbacks within it act in concert to tightly regulate intracellular cholesterol levels. Formulated using the theory of nonlinear ordinary differential equations and parameterised in the context of a hepatocyte, the governing equations are analysed numerically and analytically. Sensitivity and mathematical analysis demonstrate the importance of the two rate limiting enzymes 3-hydroxy-3-methylglutaryl-CoA reductase and squalene synthase in controlling the concentration of substrates within the pathway as well as that of cholesterol. The role of individual feedbacks, both global (between that of cholesterol and sterol regulatory element-binding protein 2; SREBP-2) and local internal (between substrates in the pathway) are investigated. We find that

Preprint ^{*}Corresponding author. Email address: m.tindall@reading.ac.uk Department of Mathematics and Statistics, University of Reading, Whiteknights, Reading, UK, RG6 6AX. Tel.: +44 118 378 8989.

Email address: m.tindall@reading.ac.uk (Marcus J. Tindall)

whilst the cholesterol SREBP-2 feedback regulates the overall system dynamics, local feedbacks activate within the pathway to tightly regulate the overall cellular cholesterol concentration. The network stability is analysed by constructing a reduced model of the full pathway and is shown to exhibit one real, stable steady-state. We close by addressing the biological question as to how farnesyl-PP levels are affected by CYP51 inhibition, and demonstrate that the regulatory mechanisms within the network work in unison to ensure they remain bounded.

16 *Keywords:* nonlinear ordinary differential equation, feedback, HMGCR,
17 squalene synthase

18 **1. Introduction**

19 The mevalonate pathway is an important metabolic pathway present in all eu-
20 karyotes, fungi and some bacteria [6, 13]. It is responsible for many processes
21 within the cell including biosynthesis of cholesterol, cell wall maintenance,
22 hormone production, protein lipidation and anchoring and is part of steroid
23 biosynthesis.

24 The body produces around 80% of cholesterol it needs [40]. A large percent-
25 age of this is synthesised by the liver via a series of reactions. In mammalian
26 cells cholesterol is a substrate for a number of other reactions [6]. Over ac-
27 cumulation of cholesterol can lead to cellular toxicity [18], whilst insufficient
28 cholesterol levels result in compromised cell structure and function. Thus
29 it is important that cholesterol levels are tightly regulated within the cell.
30 This is known as cellular cholesterol homeostasis and it works by balanc-
31 ing the influx, utilisation and efflux of cholesterol to maintain intracellular
32 concentrations within a narrow range of concentration.

33 The mevalonate pathway is comprised of two genetic synthesis cascades which
34 react with intermediate substrates to form cholesterol and has been com-
35 prehensively detailed by [22]. Sterol regulatory element-binding protein 2
36 (SREBP-2) co-regulates the gene transcription of 3-hydroxy-3-methylglutary
37 coenzyme A reductase (HMGCR) and squalene synthase. This regulation is
38 cholesterol dependent [13]. When cholesterol levels are high, SREBP-2 is
39 bound in a complex with cholesterol anchoring it to the cell membrane ren-
40 dering SREBP-2 inactive. In low cholesterol concentrations the complex

41 unbinds and through a complex series of translocation and proteolytic pro-
42 cessing steps SREBP-2 is released, relocates to the nucleus and binds to tar-
43 get DNA stimulating increased transcription leading to increased production
44 of the enzymes such as HMGCR and squalene synthase [6].

45 The central anabolic cascade of the pathway is initiated by the binding of
46 HMGCoA to the active site of HMGCR, which then catalyses its conversion
47 into mevalonate. Mevalonate is then converted to geranyl pyrophosphate
48 (geranyl-PP), farnesyl pyrophosphate (farnesyl-PP), squalene (via the inter-
49 action between farnesyl-PP and squalene synthase), lanosterol and finally
50 after some 19 further steps [11], cholesterol. A rate limiting step in this
51 chain of biosynthesis is the reduction of HMGCoA catalysed by HMGCR
52 [13].

53 The tight control of cholesterol concentration is thought possible by a number
54 of negative feedback loops that regulate HMGCR and receptors dependent
55 on intracellular cholesterol concentrations [14, 35]. Feedbacks from farnesyl-
56 PP [10] and lanosterol accelerate HMGCR degradation [4], and it has been
57 suggested that geranyl-PP plays a similar role. Cholesterol has been shown
58 to accelerate squalene synthase degradation [10] and oxygenated derivatives
59 of cholesterol have been identified in HMGCR degradation [9].

60 Many of the products formed from the mevalonate pathway are involved in
61 other cell signalling cascades. Farnesyl-PP is a major branch point in the
62 pathway which is responsible for producing six other substrates used in vital
63 cellular functions. Excessive amounts of farnesyl-PP have been suggestively
64 linked to tumours and Alzheimers disease [7, 32]. Inhibitors of the mevalonate
65 pathway are used in cardiovascular therapy (statins) and as anti-fungal agents
66 (CYP51 inhibitors) in crop protection. The extent to which altering this
67 pathway is associated with the carcinogenic and developmental effects of
68 CYP51 inhibitors has been debated [23, 26].

69 Mathematical modelling of cholesterol biosynthesis pathways has to date fo-
70 cused on specific aspects of the pathway. Kervizic and Corcos [19] developed
71 a boolean model of the pathway which focused on demonstrating the role of
72 SREBP-2 in synthesising cholesterol and the effect of statins on the process.
73 Their model showed good agreement with experimental known functioning of
74 the pathway in respect of statin applications. Watterson and colleagues [45]
75 formulated an ordinary differential equation (ODE) model of the pathway
76 to understand the effect of the immune response and statins on the overall

77 pathway. Using experimental data from macrophages, their work shows the
78 gradual reduction in pathway activity as a result of the innate immune re-
79 sponse, versus the more step like change imparted by statins. A recent paper
80 by Bhattacharya et al. [2] formulated and analysed a three variable nonlin-
81 ear ODE simplified model of the pathway that incorporates a description of
82 HMGCR mRNA, HMGCR protein and cholesterol biosynthesis. The syn-
83 thesis of HMGCR mRNA is controlled by a negative feedback loop, whereby
84 cholesterol is able to bind to free SREBP-2. Model results and analysis
85 demonstrate the system exhibits one real stable steady-state which is mono-
86 tonic, periodic or damped periodic under certain model parameterisations as
87 a result of cholesterol's negative regulation of SREBP-2.

88 In this paper we seek here to expand our knowledge of cholesterol biosynthesis
89 by deriving and solving a nonlinear ODE model of the mevalonate choles-
90 terol biosynthesis pathway. Our aim is to better understand the role of the
91 overall network structure in dynamically regulating cholesterol biosynthesis,
92 in particular that of multiple synthesis pathways and feedbacks. We begin in
93 Section 2 by presenting our main model of the pathway which incorporates
94 the core regulation mechanisms and feedbacks within the signalling cascade.
95 An ODE model of the pathway is derived from first principles in Section 3,
96 which is subsequently parameterised and solved numerically in Section 4.
97 The results of a local sensitivity analysis are presented in Section 5 and the
98 role of the second rate limiting step in the pathway between farnesyl-PP
99 and squalene synthase is analysed in detail in Section 6. The effect of the
100 numerous feedbacks within the pathway are analysed in Section 9 before a
101 steady-state stability analysis of a model reduction of the full network model
102 is presented in Section 7. Negative feedbacks may lead to a network ex-
103 hibiting oscillatory type behaviour and as such we examine whether such
104 solutions may be observed for certain parameterisations of the full model in
105 Section 8. We test the hypothesis that the application of CYP51 inhibitors
106 leads to increased levels of farnesyl-PP, via inhibition of cholesterol produc-
107 tion following that of lanosterol, in Section 10. Our results and conclusions
108 are discussed in Section 11.

109 **2. The Mevalonate Pathway**

110 Given the complexity of the full pathway we consider here a reduction, in-
111 corporating the details outlined in the Introduction, which captures the core

112 synthesis processes, feedbacks and branch points associated with cholesterol
113 regulation as shown in Figure 1. Essentially, substrates and enzymes that
114 form sequential linear steps in the pathway and which are not involved in
115 feedbacks or branch points, have been omitted. This leaves three core as-
116 pects:

- 117 1. the two genetic transcriptional control pathways of HMGCR and squalene
118 synthase by SREBP-2;
- 119 2. the central metabolic cascade which synthesises intermediary mevalonate
120 products and sterols with controlling steps using the enzymes
121 HMGCR and squalene synthase; and
- 122 3. negative feedback controls, including negative regulation of SREBP-2
123 by cholesterol and the concentration dependent feedbacks from sterol
124 and non-sterol products affecting the HMGCR and squalene synthase
125 degradation rates.

126 In high cholesterol concentrations SREBP-2 is bound to a cholesterol molecule
127 anchoring it to the intracellular membrane, represented in Figure 1 by the
128 $\bar{\kappa}_3/\bar{\kappa}_{-3}$ negative feedback. Here $\bar{\kappa}_3$ represents the association reaction, whilst
129 $\bar{\kappa}_{-3}$ the disassociation reaction. In low cholesterol concentrations, SREBP-2
130 disassociates from the cholesterol molecule allowing it, via a series of inter-
131 mediate steps, to produce an active transcription factor that relocates to the
132 nucleus to act upon the DNA stimulating endogenous production of HMGCR
133 and squalene synthase. This is represented in Figure 1, by the two reactions
134 $\bar{\kappa}_1/\bar{\kappa}_{-1}$, through $\bar{\mu}_1$ to $\bar{\mu}_3$ and $\bar{\kappa}_2/\bar{\kappa}_{-2}$, through $\bar{\mu}_2$ to $\bar{\mu}_4$. In the centre of the
135 pathway HMGCR binds with HMGCoA to form an intermediary complex
136 which leads to mevalonate production. This is subsequently phosphorylated
137 twice then converted to isopentenyl-PP and geranyl-PP. In Figure 1 these
138 five steps are represented as $\bar{\mu}_5$. From geranyl-PP, farnesyl-PP is produced.
139 It is at this point that squalene synthase reacts with farnesyl-PP and this
140 complex produces squalene. Squalene produces squalene-2,3-epoxide after
141 which lanosterol is formed. We represent these two steps by $\bar{\mu}_8$. There are a
142 further 19 reactions from lanosterol until cholesterol [11] which we approxi-
143 mate by the parameter $\bar{\mu}_9$. This approximation allows for the simplification
144 of an otherwise already under parameterised system.

145 There are a number of feedbacks within the pathway shown in Figure 1.
146 Goldstein and Brown [4] found that sterols caused a negative feedback on
147 HMGCR production but hypothesised sterols were not the only inhibitors.

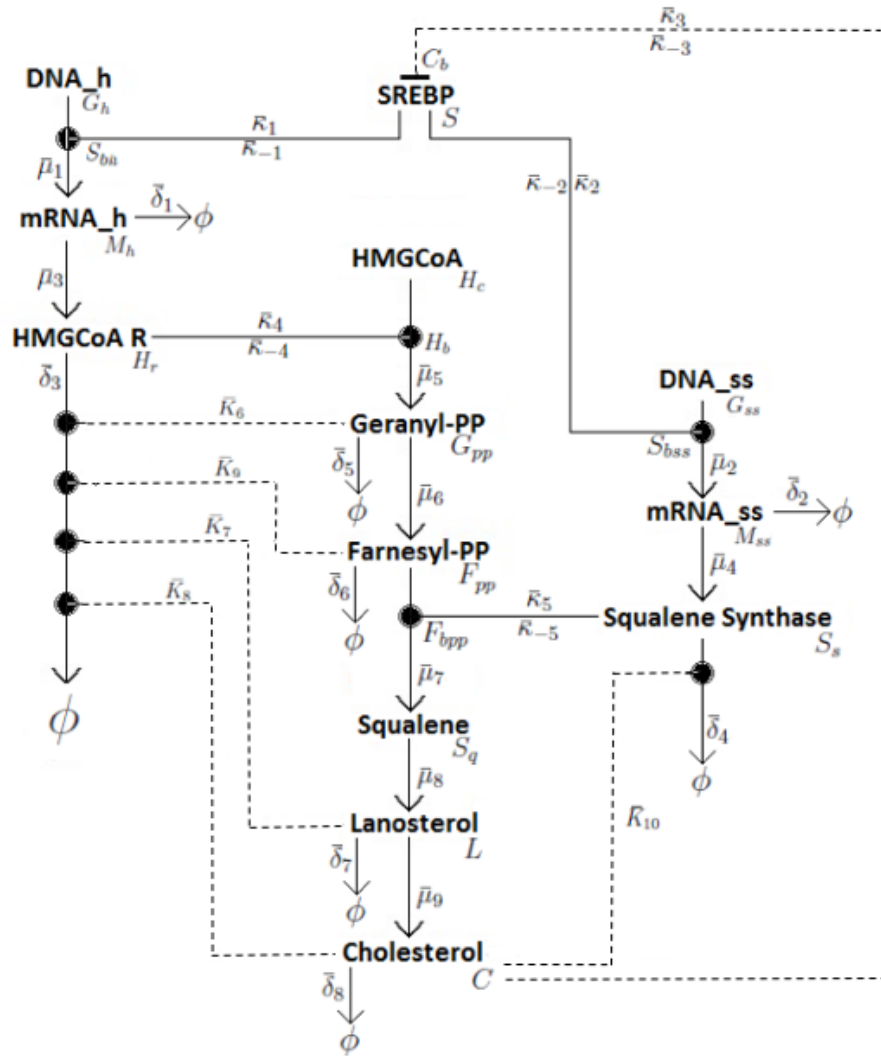


Figure 1: A simplified model of the mevalonate pathway. Arrows show forward reactions, circles show stimulative reactions and horizontal bars indicate inhibition. Here ϕ indicates the removal of a product from the pathway, either by degradation or use in another process. There are three main focal points to the pathway; the two genetic pathways of HMGCR and squalene synthase, the central metabolic cascade and the regulatory feedbacks (dashed lines).

148 Hence we have concentration dependent feedbacks from lanosterol (\bar{K}_7) and
 149 cholesterol (\bar{K}_8) that up-regulate the degradation of HMGCR. It has been
 150 suggested that geranyl-PP also up-regulates HMGCR degradation [14] (\bar{K}_6)
 151 and recent findings by Foresti et al. [10] have shown farnesyl-PP is linked to
 152 HMGCR degradation (\bar{K}_9). Foresti et al. also show a similar concentration
 153 dependent reaction between cholesterol and the rate of squalene synthase
 154 degradation (\bar{K}_{10}).

155 3. Mathematical model

156 In this section we derive a system of non-linear ODEs to describe the reaction
 157 network detailed in Section 2 using the law of mass action. Details on the
 158 biochemistry underlying each step within the pathway are given in Appendix
 159 A. Applying the law of mass action to equations (A.1) - (A.6) gives

$$\frac{d\bar{g}_h}{dt} = \bar{\kappa}_{-1}\bar{s}_{bh} - \bar{\kappa}_1\bar{s}^{x_h}\bar{g}_h, \quad (1)$$

$$\frac{d\bar{g}_{ss}}{dt} = \bar{\kappa}_{-2}\bar{s}_{bss} - \bar{\kappa}_2\bar{s}^{x_s}\bar{g}_{ss}, \quad (2)$$

$$\frac{d\bar{s}}{dt} = x_h\bar{\kappa}_{-1}\bar{s}_{bh} - x_h\bar{\kappa}_1\bar{s}^{x_h}\bar{g}_h + x_s\bar{\kappa}_{-2}\bar{s}_{bss} - x_s\bar{\kappa}_2\bar{s}^{x_s}\bar{g}_{ss} - \bar{\kappa}_3\bar{c}^{x_c}\bar{s} + \bar{\kappa}_{-3}\bar{c}_b, \quad (3)$$

$$\frac{d\bar{s}_{bh}}{dt} = -\bar{\kappa}_{-1}\bar{s}_{bh} + \bar{\kappa}_1\bar{s}^{x_h}\bar{g}_h, \quad (4)$$

$$\frac{d\bar{s}_{bss}}{dt} = -\bar{\kappa}_{-2}\bar{s}_{bss} + \bar{\kappa}_2\bar{s}^{x_s}\bar{g}_{ss}, \quad (5)$$

$$\frac{d\bar{m}_h}{dt} = \bar{\mu}_1\bar{s}_{bh} - \bar{\delta}_1\bar{m}_h, \quad (6)$$

$$\frac{d\bar{m}_{ss}}{dt} = \bar{\mu}_2\bar{s}_{bss} - \bar{\delta}_2\bar{m}_{ss}, \quad (7)$$

$$\begin{aligned} \frac{d\bar{h}_r}{dt} = & \bar{\mu}_3\bar{m}_h + \bar{\kappa}_{-4}\bar{h}_b - \bar{\kappa}_4\bar{h}_r\bar{h}_c + \bar{\mu}_5\bar{h}_b \\ & - \bar{\delta}_3\bar{h}_r \left(1 + \delta_{hg} \frac{\bar{g}_{pp}}{\bar{g}_{pp} + \bar{K}_6} + \delta_{hf} \frac{\bar{f}_{pp}}{\bar{f}_{pp} + \bar{K}_9} + \delta_{hl} \frac{\bar{l}}{\bar{l} + \bar{K}_7} + \delta_{hc} \frac{\bar{c}}{\bar{c} + \bar{K}_8} \right), \end{aligned} \quad (8)$$

$$\frac{d\bar{s}_s}{dt} = \bar{\mu}_4\bar{m}_{ss} + \bar{\kappa}_{-5}\bar{f}_{bpp} - \bar{\kappa}_5\bar{s}_s\bar{f}_{pp}^2 + \bar{\mu}_7\bar{f}_{bpp} - \bar{\delta}_4\bar{s}_s \left(1 + \delta_{sc} \frac{\bar{c}}{\bar{c} + \bar{K}_{10}} \right), \quad (9)$$

$$\frac{d\bar{h}_c}{d\bar{t}} = \bar{\kappa}_{-4}\bar{h}_b - \bar{\kappa}_4\bar{h}_r\bar{h}_c + \bar{\omega}, \quad (10)$$

$$\frac{d\bar{h}_b}{d\bar{t}} = -\bar{\kappa}_{-4}\bar{h}_b + \bar{\kappa}_4\bar{h}_r\bar{h}_c - \bar{\mu}_5\bar{h}_b - \bar{\delta}_3\bar{h}_b, \quad (11)$$

$$\frac{d\bar{g}_{pp}}{d\bar{t}} = \bar{\mu}_5\bar{h}_b - \bar{\delta}_5\bar{g}_{pp} - \bar{\mu}_6\bar{g}_{pp}, \quad (12)$$

$$\frac{d\bar{f}_{pp}}{d\bar{t}} = \bar{\mu}_6\bar{g}_{pp} - \bar{\delta}_6\bar{f}_{pp} - 2\bar{\kappa}_5\bar{s}_s\bar{f}_{pp}^2 + 2\bar{\kappa}_{-5}\bar{f}_{bpp}, \quad (13)$$

$$\frac{d\bar{f}_{bpp}}{d\bar{t}} = \bar{\kappa}_5\bar{s}_s\bar{f}_{pp}^2 - \bar{\kappa}_{-5}\bar{f}_{bpp} - \bar{\mu}_7\bar{f}_{bpp} - \bar{\delta}_4\bar{f}_{bpp}, \quad (14)$$

$$\frac{d\bar{s}_q}{d\bar{t}} = \bar{\mu}_7\bar{f}_{bpp} - \bar{\mu}_8\bar{s}_q, \quad (15)$$

$$\frac{d\bar{l}}{d\bar{t}} = \bar{\mu}_8\bar{s}_q - \bar{\delta}_7\bar{l} - \bar{\mu}_9\bar{l}, \quad (16)$$

$$\frac{d\bar{c}}{d\bar{t}} = \bar{\mu}_9\bar{l} - \bar{\delta}_8\bar{c} + x_c\bar{\kappa}_{-3}\bar{c}_b - x_c\bar{\kappa}_3\bar{c}^{x_c}\bar{s}, \quad (17)$$

$$\frac{d\bar{c}_b}{d\bar{t}} = \bar{\kappa}_3\bar{c}^{x_c}\bar{s} - \bar{\kappa}_{-3}\bar{c}_b, \quad (18)$$

161 where, with square brackets denoting concentration,

$$\begin{aligned} \bar{g}_h &= [G_h], & \bar{g}_{ss} &= [G_{ss}], & \bar{s} &= [S], & \bar{s}_{bh} &= [S_{bh}], & \bar{s}_{bss} &= [S_{bss}], \\ \bar{m}_h &= [M_h], & \bar{m}_{ss} &= [M_{ss}], & \bar{h}_r &= [H_r], & \bar{s}_s &= [S_s], & \bar{h}_c &= [H_c], \\ \bar{h}_b &= [H_b], & \bar{g}_{pp} &= [G_{pp}], & \bar{f}_{pp} &= [F_{pp}], & \bar{f}_{bpp} &= [F_{bpp}], & \bar{s}_q &= [S_q], \\ & & \bar{l} &= [L], & \bar{c} &= [C], & \text{and} & \bar{c}_b &= [C_b], \end{aligned}$$

162 and the system is closed with the initial conditions

$$\begin{aligned} \bar{g}_h(0) &= \bar{g}_{h0}, & \bar{g}_s(0) &= \bar{g}_{s0}, & \bar{s}(0) &= \bar{s}_0, & \bar{s}_{bh}(0) &= 0, & \bar{s}_{bss}(0) &= 0, \\ \bar{m}_h(0) &= \bar{m}_{h0}, & \bar{m}_{ss}(0) &= \bar{m}_{ss0}, & \bar{h}_r(0) &= \bar{h}_{r0}, & \bar{s}_s(0) &= \bar{s}_{s0}, \\ \bar{h}_c(0) &= \bar{h}_{c0}, & \bar{h}_b(0) &= 0, & \bar{g}_{pp}(0) &= 0, & \bar{f}_{pp}(0) &= 0, & \bar{f}_{bpp}(0) &= 0, \\ \bar{s}_q(0) &= 0, & \bar{l}(0) &= 0, & \bar{c}(0) &= 0 & \text{and} & \bar{c}_b(0) &= 0, \end{aligned} \quad (19)$$

163 at $\bar{t} = 0$

164 Many of the initial conditions are assumed equal to zero in order to under-
165 stand the overall dynamical response of the system. The feedbacks acting

166 on HMGCR and squalene synthase degradation, equations (22) and (23) re-
 167 spectively, are dependent on geranyl-PP, farnesyl-PP, lanosterol and choles-
 168 terol concentrations. We thus assume these follow sigmoidal shape kinet-
 169 ics [24], where $\bar{K}_{6,7,8,9,10}$ are the respective Michaelis-Menten constants and
 170 $\delta_{hg}, \delta_{hf}, \delta_{hl}$ and δ_{hc} , are dimensionless weighting constants representing the
 171 additional effect of geranyl-PP, farnesyl-PP, lanosterol and cholesterol to that
 172 of the natural rate of HMGCR degradation, respectively, and δ_{sc} is that of a
 173 similar effect of cholesterol on the natural decay rate of squalene synthase.

174 By invoking conservation of certain entities within the pathway and employ-
 175 ing quasi-equilibrium approximations (see Appendix B) equations (1) to (17)
 176 are reduced to

$$\frac{d\bar{m}_h}{d\bar{t}} = \frac{\bar{\mu}_1}{1 + \left(\frac{\bar{K}_1(1+(\frac{\bar{c}}{\bar{K}_3})^{x_c})}{\bar{s}_0} \right)^{x_h}} - \bar{\delta}_1 \bar{m}_h, \quad (20)$$

$$\frac{d\bar{m}_{ss}}{d\bar{t}} = \frac{\bar{\mu}_2}{1 + \left(\frac{\bar{K}_2(1+(\frac{\bar{c}}{\bar{K}_3})^{x_c})}{\bar{s}_0} \right)^{x_s}} - \bar{\delta}_2 \bar{m}_{ss}, \quad (21)$$

$$\begin{aligned} \frac{d\bar{h}_r}{d\bar{t}} = & \bar{\mu}_3 \bar{m}_h + \bar{\kappa}_{-4} \bar{h}_b - \bar{\kappa}_4 \bar{h}_r \bar{h}_c + \bar{\mu}_5 \bar{h}_b \\ & - \bar{\delta}_3 \bar{h}_r \left(1 + \delta_{hg} \frac{\bar{g}_{pp}}{\bar{g}_{pp} + \bar{K}_6} + \delta_{hf} \frac{\bar{f}_{pp}}{\bar{f}_{pp} + \bar{K}_9} + \delta_{hl} \frac{\bar{l}}{\bar{l} + \bar{K}_7} + \delta_{hc} \frac{\bar{c}}{\bar{c} + \bar{K}_8} \right), \end{aligned} \quad (22)$$

$$\frac{d\bar{s}_s}{d\bar{t}} = \bar{\mu}_4 \bar{m}_{ss} + \bar{\kappa}_{-5} \bar{f}_{bpp} - \bar{\kappa}_5 \bar{s}_s \bar{f}_{pp}^2 + \bar{\mu}_7 \bar{f}_{bpp} - \bar{\delta}_4 \bar{s}_s \left(1 + \delta_{sc} \frac{\bar{c}}{\bar{c} + \bar{K}_{10}} \right), \quad (23)$$

$$\frac{d\bar{h}_c}{d\bar{t}} = \bar{\kappa}_{-4} \bar{h}_b - \bar{\kappa}_4 \bar{h}_r \bar{h}_c + \bar{\omega}, \quad (24)$$

$$\frac{d\bar{h}_b}{d\bar{t}} = -\bar{\kappa}_{-4} \bar{h}_b + \bar{\kappa}_4 \bar{h}_r \bar{h}_c - \bar{\mu}_5 \bar{h}_b - \bar{\delta}_3 \bar{h}_b, \quad (25)$$

$$\frac{d\bar{g}_{pp}}{d\bar{t}} = \bar{\mu}_5 \bar{h}_b - \bar{\delta}_5 \bar{g}_{pp} - \bar{\mu}_6 \bar{g}_{pp}, \quad (26)$$

$$\frac{d\bar{f}_{pp}}{d\bar{t}} = \bar{\mu}_6 \bar{g}_{pp} - \bar{\delta}_6 \bar{f}_{pp} - 2\bar{\kappa}_5 \bar{s}_s \bar{f}_{pp}^2 + 2\bar{\kappa}_{-5} \bar{f}_{bpp}, \quad (27)$$

$$\frac{d\bar{f}_{bpp}}{d\bar{t}} = \bar{\kappa}_5 \bar{s}_s \bar{f}_{pp}^2 - \bar{\kappa}_{-5} \bar{f}_{bpp} - \bar{\mu}_7 \bar{f}_{bpp} - \bar{\delta}_4 \bar{f}_{bpp}, \quad (28)$$

$$\frac{d\bar{s}_q}{d\bar{t}} = \bar{\mu}_7 \bar{f}_{bpp} - \bar{\mu}_8 \bar{s}_q, \quad (29)$$

$$\frac{d\bar{l}}{d\bar{t}} = \bar{\mu}_8 \bar{s}_q - \bar{\delta}_7 \bar{l} - \bar{\mu}_9 \bar{l}, \quad (30)$$

$$\frac{d\bar{c}}{d\bar{t}} = \frac{\bar{\mu}_9 \bar{l} - \bar{\delta}_8 \bar{c}}{1 - x_c(\bar{s}' + x_h \bar{s}'_{bh} + x_s \bar{s}'_{bss})}, \quad (31)$$

178 where \bar{s}'_{bss} , \bar{s}'_{bh} and \bar{s}' are given by equations (B.9), (B.10) and (B.8) respec-
 179 tively, and $'$ indicates differentiation with respect to \bar{c} . The initial conditions
 180 are given by

$$\begin{aligned} \bar{m}_h(0) &= \bar{m}_{h0}, & \bar{m}_{ss}(0) &= \bar{m}_{ss0}, & \bar{h}_r(0) &= \bar{h}_{r0}, & \bar{s}_s(0) &= \bar{s}_{s0}, \\ \bar{h}_c(0) &= \bar{h}_{c0}, & \bar{h}_b(0) &= 0, & \bar{g}_{pp}(0) &= 0, & \bar{f}_{pp}(0) &= 0, & \bar{f}_{bpp}(0) &= 0, \\ \bar{s}_q(0) &= 0, & \bar{l}(0) &= 0 & \text{and} & \bar{c}(0) &= 0. \end{aligned} \quad (32)$$

181 3.1. Non-dimensionalisation

182 Equations (20) to (32) are non-dimensionalised according to the following
 183 rescalings

$$\begin{aligned} \bar{t} &= \frac{t}{\delta_7}, & \bar{m}_h &= \bar{m}_{h0} m_h, & \bar{m}_{ss} &= \bar{m}_{h0} m_{ss}, & \bar{h}_r &= \bar{s}_{sT} h_r, \\ \bar{S}_s &= \bar{s}_{sT} s_s, & \bar{h}_c &= \bar{h}_{cT} h_c, & \bar{h}_b &= \bar{h}_{cT} h_b, & \bar{g}_{pp} &= \bar{h}_{cT} g_{pp}, \\ \bar{f}_{pp} &= \bar{h}_{cT} f_{pp}, & \bar{f}_{bpp} &= \bar{h}_{cT} f_{bpp}, & \bar{s}_q &= \bar{h}_{cT} s_q, & \bar{l} &= \bar{h}_{cT} l, & \bar{c} &= \bar{h}_{cT} c, \end{aligned} \quad (33)$$

184 where \bar{s}_{sT} and \bar{h}_{cT} are the experimentally determined total concentrations of
 185 squalene synthase and HMG-CoA in a resting hepatocyte cell [5]. Substitut-

186 ing these rescalings into equations (20) through (32), we obtain

$$\frac{dm_h}{dt} = \frac{\mu_1}{1 + \left(\kappa_1 \left(1 + \left(\frac{c}{\kappa_3}\right)^{x_c}\right)\right)^{x_h}} - \delta_1 m_h, \quad (34)$$

$$\frac{dm_{ss}}{dt} = \frac{\mu_2}{1 + \left(\kappa_2 \left(1 + \left(\frac{c}{\kappa_3}\right)^{x_c}\right)\right)^{x_s}} - \delta_2 m_{ss}, \quad (35)$$

$$\begin{aligned} \frac{dh_r}{dt} = & \mu_3 m_h + \kappa_{-4} \alpha h_b - \kappa_4 \alpha h_r h_c + \mu_5 \alpha h_b \\ & - \delta_3 h_r \left(1 + \delta_{hg} \frac{g_{pp}}{g_{pp} + K_6} + \delta_{hf} \frac{f_{pp}}{f_{pp} + K_9} + \delta_{hl} \frac{l}{l + K_7} + \right. \\ & \left. \delta_{hc} \frac{c}{c + K_8} \right), \end{aligned} \quad (36)$$

187

$$\begin{aligned} \frac{ds_s}{dt} = & \mu_4 m_{ss} + \kappa_{-5} \alpha f_{bpp} - \kappa_5 \alpha s_s f_{pp}^2 + \mu_7 \alpha f_{bpp} - \\ & \delta_4 s_s \left(1 + \delta_{sc} \frac{c}{c + K_{10}} \right), \end{aligned} \quad (37)$$

$$\frac{dh_c}{dt} = \kappa_{-4} h_b - \kappa_4 h_r h_c + \omega, \quad (38)$$

$$\frac{dh_b}{dt} = -\kappa_{-4} h_b + \kappa_4 h_r h_c - \mu_5 h_b - \delta_3 h_b, \quad (39)$$

$$\frac{dg_{pp}}{dt} = \mu_5 h_b - \delta_5 g_{pp} - \mu_6 g_{pp}, \quad (40)$$

$$\frac{df_{pp}}{dt} = \mu_6 g_{pp} - \delta_6 f_{pp} - 2\kappa_5 s_s f_{pp}^2 + 2\kappa_{-5} f_{bpp}, \quad (41)$$

$$\frac{df_{bpp}}{dt} = \kappa_5 s_s f_{bpp}^2 - \kappa_{-5} f_{bpp} - \mu_7 f_{bpp} - \delta_4 f_{bpp}, \quad (42)$$

$$\frac{ds_q}{dt} = \mu_7 f_{bpp} - \mu_8 s_q, \quad (43)$$

$$\frac{dl}{dt} = \mu_8 s_q - \delta_7 l - \mu_9 l, \quad (44)$$

$$\frac{dc}{dt} = \frac{\mu_9 l - \delta_8 c}{1 - x_c (s_0 s' + x_h g_{h0} s'_{bh} + x_s g_{ss0} s'_{bss})}, \quad (45)$$

188 with the non-dimensional initial conditions, at $t = 0$, given by

$$\begin{aligned} m_h(0) = 1, \quad m_{ss}(0) = 1, \quad h_r(0) = 0, \quad s_s(0) = 0, \quad h_c(0) = 0, \\ h_b(0) = 0, \quad g_{pp}(0) = 0, \quad f_{pp}(0) = 0, \quad f_{bpp}(0) = 0, \quad s_q(0) = 0, \\ l(0) = 0 \quad \text{and} \quad c(0) = 0, \end{aligned} \tag{46}$$

189 and the non-dimensional parameters summarised in Table 2.

190 *3.2. Model parameterisation*

191 Wherever possible data from human liver (hepatocyte G2; HepG2) cells
192 was used to inform our parameter values. Where values have been unavail-
193 able from HepG2 cells, other sources have included human liver microsomes
194 (pieces of the endoplasmic reticulum used in some experimental work) or Chi-
195 nese hamster ovary cells. Details regarding the estimation of all parameter
196 values is provided in Appendix C, whilst Table 1 summarises each dimen-
197 sional parameter, their value and source. Non-dimensional parameters are
198 stated in Table 2.

199 In cases where no information was available, approximations were first made
200 based on similar occurring reactions and processes, e.g. rates of mRNA
201 degradation, as detailed in Appendix C. For instance, rates calculated from
202 Bhattacharya et al. [2] regarding HMGCR and cholesterol synthesis, specif-
203 ically binding affinities and degradation rates relating to HMGCR mRNA,
204 HMGCR and cholesterol, were used to initially inform rates corresponding
205 to squalene synthase synthesis and degradation as well as (non)sterol pro-
206 duction rates. Using Matlab [21] the model was then simulated numerically
207 (using the ode15s solver) and analysed via a local sensitivity analysis (coded
208 directly into Matlab). The sensitivity analysis was used to ascertain the
209 importance of the unknown assumed parameter values in affecting the to-
210 tal cholesterol concentration in an heptaocyte. Based on the findings of this
211 analysis, parameter values were then adjusted accordingly (as detailed in Ap-
212 pendix C) to ensure the model reproduced previously determined cholesterol
213 concentrations [2].

214 In the absence of any available data in other cell systems with which to
215 compare any determined values, the additional effects of farnesyl-PP, geranyl-
216 PP, lanosterol and cholesterol on HMGCR degradation and cholesterol on

217 that of squalene synthase degradation (δ_{hg} , δ_{hf} , δ_{hl} , δ_{hc} , δ_{sc}) were set equal
 218 to unity.

219 It is important to note that the utilisation of cholesterol and farnesyl-PP can
 220 vary depending on other intracellular processes. To simplify our model, we
 221 have assumed a constant value of cholesterol and farnesyl-PP degradation to
 222 include cellular utilisation, based on the work by Bhattacharya et al. [2].

Table 1: Dimensional parameters. Here “Param.” denotes parameter, “molec” molecules, “SqS” squalene synthase.

Param.	Description	Value	Units	Reference
\bar{m}_{h0}	Initial HMGCR mRNA concentration.	3.0×10^9	molec./ml	[30]
\bar{m}_{ss0}	Initial SqS mRNA concentration.	3.0×10^9	molec./ml	[30]
\bar{s}_sT	Total SqS synthase concentration.	7.59×10^{14}	molec./ml	[5]
\bar{h}_cT	Total HMGC _o A concentration.	1.98×10^{15}	molec./ml	[33, 38]
\bar{s}_0	Total SREBP-2 concentration.	8.21×10^{16}	molec./ml	[31, 2]
\bar{g}_{h0}	HMGCR gene concentration.	2.11×10^9	molec./ml	[41]/This study.
\bar{g}_{ss0}	SqS gene concentration.	2.11×10^9	molec./ml	This study.
$\bar{\mu}_1^*$	HMGCR transcription.	5.17×10^5	$\frac{\text{molec.}}{\text{ml.s}}$	[8, 12]
$\bar{\mu}_2^*$	SqS transcription.	4.65×10^5	$\frac{\text{molec.}}{\text{ml.s}}$	[8, 37]
$\bar{\mu}_3$	HMGCR translation	3.32×10^{-2}	1/s	[39, 17]
$\bar{\mu}_4$	SqS translation.	1.91×10^{-2}	1/s	[39, 36]
$\bar{\mu}_5$	Geranyl-PP formation.	4.33×10^{-2}	1/s	[15, 33, 43]
$\bar{\mu}_6$	Farnesyl-PP formation.	4.33×10^{-2}	1/s	[15, 33, 47]
$\bar{\mu}_7$	SqS formation.	2.17×10^{-1}	1/s	This study.
$\bar{\mu}_8$	Lanosterol formation.	4.33×10^{-2}	1/s	[15, 33, 47]
$\bar{\mu}_9$	Cholesterol formation.	4.33×10^{-2}	1/s	[15, 33, 47]
\bar{K}_1	SREBP-2-HMGCR gene binding affinity.	8.21×10^{12}	molec./ml	[29]/This study.
\bar{K}_2	SREBP-2-SqS gene binding affinity.	8.21×10^{12}	molec./ml	[29]/This study.
\bar{K}_3	Cholesterol-SREBP-2 disassociation constant.	1.49×10^{16}	molec./ml	[46]/This study.
$\bar{\kappa}_4$	HMGCR-HMGC _o A association.	1.39×10^{-16}	$\frac{\text{ml}}{\text{molec.s}}$	This study.

Table 1 – continued

$\bar{\kappa}_{-4}$	HMGCR-HMGCoA disassociation.	1.75×10^{-7}	1/s	This study
$\bar{\kappa}_5$	SqS - Farnesyl-PP association.	1.76×10^{-30}	$\frac{\text{ml}^2}{\text{molec}^2 \cdot \text{s}}$	This study
$\bar{\kappa}_{-5}$	SqS - Farnesyl-PP disassociation.	1.75×10^{-5}	1/s	This study.
\bar{K}_6	Michaelis-Menten constant for geranyl-PP/HMGCR degradation.	5.00×10^9	molec./ml	This study.
\bar{K}_7	Michaelis-Menten constant for lanosterol/HMGCR degradation.	5.00×10^{12}	molec./ml	This study.
\bar{K}_8	Michaelis-Menten constant for cholesterol/HMGCR degradation.	5.00×10^{17}	molec./ml	This study.
\bar{K}_9	Michaelis-Menten constant for farnesyl-PP/HMGCR degradation.	5.00×10^{11}	molec./ml	This study.
\bar{K}_{10}	Michaelis-Menten constant for cholesterol/SqS degradation.	5.00×10^{17}	molec./ml	This study.
$\bar{\delta}_1$	HMGCR mRNA degradation.	4.48×10^{-5}	1/s	[3]
$\bar{\delta}_2$	SqS mRNA degradation.	4.48×10^{-5}	1/s	This study.
$\bar{\delta}_3$	HMGCR degradation.	6.42×10^{-5}	1/s	[44]
$\bar{\delta}_4$	SqS degradation.	6.42×10^{-5}	1/s	This study.
$\bar{\delta}_5$	Geranyl-PP degradation.	1.20×10^{-4}	1/s	This study.
$\bar{\delta}_6$	Farnesyl-PP degradation.	1.20×10^{-4}	1/s	This study.
$\bar{\delta}_7$	Lanosterol degradation.	1.20×10^{-4}	1/s	This study.
$\bar{\delta}_8$	Cholesterol degradation.	1.20×10^{-4}	1/s	[2]
δ_{hg}	Additional effect of geranyl-PP on HMGCR degradation.	1	-	This study
δ_{hf}	Additional effect of farnesyl-PP on HMGCR degradation.	1	-	This study
δ_{hl}	Additional effect of lanosterol on HMGCR degradation.	1	-	This study
δ_{hc}	Additional effect of cholesterol on HMGCR degradation.	1	-	This study
δ_{sc}	Additional effect of cholesterol on SqS degradation.	1	-	This study
$\bar{\omega}$	HMGCoA production.	3.90×10^{11}	molec./ml	This study.
x_h	Binding sites on HMGCR	3	-	[28]

Table 1 – continued

x_s	gene for SREBP-2. Binding sites on SqS gene for SREBP-2.	1	-	This study.
x_c	Molecules of cholesterol to inactivate SREBP-2.	4	-	[46, 16]

Table 2: Table of non-dimensional parameters, their relation to dimensional ones and value.

Parameter	Description	Definition	Value
s_0	Ratio of SREBP-2 to HMGCoA	\bar{s}_0/h_{cT}	41.46
g_{h0}	Ratio of HMGCR gene to SREBP-2	\bar{g}_{h0}/\bar{s}_0	2.57×10^{-8}
g_{ss0}	Ratio of SqS gene to SREBP-2	\bar{g}_{ss0}/\bar{s}_0	2.57×10^{-8}
μ_1	HMGCR mRNA transcription.	$\frac{\mu_1^*}{\delta_7 \bar{m}_{h0}}$	1.44
μ_2	SqS mRNA transcription.	$\frac{\mu_2^*}{\delta_7 \bar{m}_{h0}}$	1.29
μ_3	HMGCR translation.	$\frac{\mu_3^* \bar{m}_{h0}}{\delta_7 \bar{m}_{h0}}$	1.10×10^{-3}
μ_4	SqS translation.	$\frac{\mu_4^* \bar{m}_{h0}}{\delta_7 \bar{m}_{h0}}$	6.29×10^{-4}
μ_5	Geranyl-PP production.	$\frac{\mu_5}{\delta_7}$	3.61×10^2
μ_6	Farnesyl-PP production.	$\frac{\mu_6}{\delta_7}$	3.61×10^2
μ_7	SqS production.	$\frac{\mu_7}{\delta_7}$	1.80×10^3
μ_8	Lanosterol production.	$\frac{\mu_8}{\delta_7}$	3.61×10^2
μ_9	Cholesterol production.	$\frac{\mu_9}{\delta_7}$	3.61×10^2
κ_1	SREBP-2-HMGCR gene binding affinity.	$\frac{K_1}{\bar{s}_0}$	1×10^{-4}
κ_2	SREBP-2-SqS gene binding affinity.	$\frac{K_2}{\bar{s}_0}$	1×10^{-4}
κ_3	Cholesterol-SREBP-2 dissociation constant.	$\frac{K_3}{h_{cT}}$	7.5
κ_4	HMGCR-HMGCoA association.	$\frac{\bar{\kappa}_4 \bar{s}_s T}{\delta_7}$	8.83×10^2
κ_{-4}	HMGCR-HMGCoA disassociation.	$\frac{\bar{\kappa}_{-4}}{\delta_7}$	1.46×10^{-3}
κ_5	SqS-farnesyl-PP association.	$\frac{\bar{\kappa}_5 h_{cT} \bar{s}_s T}{\delta_7}$	2.20×10^4
κ_{-5}	SqS-farnesyl-PP disassociation.	$\frac{\bar{\kappa}_{-5}}{\delta_7}$	1.46×10^{-1}
K_6	Michaelis-Menten constant for geranyl-PP/HMGCR degradation.	$\frac{K_6}{h_{cT}}$	2.53×10^{-6}
K_7	Michaelis-Menten constant for lanosterol/HMGCR degradation.	$\frac{K_7}{h_{cT}}$	2.53×10^{-3}
K_8	Michaelis-Menten constant for cholesterol/HMGCR degradation.	$\frac{K_8}{h_{cT}}$	2.53×10^2
K_9	Michaelis-Menten constant	$\frac{K_9}{h_{cT}}$	2.53×10^{-4}

Table 2 – continued

K_{10}	for farnesyl-PP/HMGCR degradation. Michaelis-Menten constant for cholesterol/SqS degradation.	$\frac{\bar{K}_{10}}{h_{cT}}$	2.53×10^2
δ_1	HMGCR mRNA degradation.	$\frac{\delta_1}{\delta_7}$	3.73×10^{-1}
δ_2	SqS mRNA degradation.	$\frac{\delta_2}{\delta_7}$	3.73×10^{-1}
δ_3	HMGCR degradation.	$\frac{\delta_3}{\delta_7}$	5.35×10^{-1}
δ_4	SqS degradation.	$\frac{\delta_4}{\delta_7}$	5.35×10^{-1}
δ_5	Geranyl-PP degradation.	$\frac{\delta_5}{\delta_7}$	1
δ_6	Farnesyl-PP degradation.	$\frac{\delta_6}{\delta_7}$	1
δ_7	Lanosterol degradation.	$\frac{\delta_7}{\delta_7}$	1
δ_8	Cholesterol degradation.	$\frac{\delta_8}{\delta_7}$	1
ω	HMGCoA production.	$\frac{\omega}{\delta_7 h_{c0}}$	0.82
α	Ratio of total HMGCoA to SqS.	$\frac{h_{cT}}{\bar{s}_s T}$	2.61

223 4. Analysis of numerical results

224 In this section we present numerical solutions to equations (34) to (46), pa-
 225 rameterised by Table 2, obtained using the MATLAB stiff differential equa-
 226 tion solver ode15s [21]. Results are shown in Figure 2. Time has been re-
 227 dimensionalised on the x -axis and simulations run until the system reaches
 228 steady-state.

229 Figure 2 shows the initial increase of HMGCR and squalene synthase mRNA;
 230 a result of no cholesterol being initially present in the system. HMGCR and
 231 squalene synthase mRNA transcription subsequently leads to their transla-
 232 tion into their respective proteins. As HMGCR increases it binds to HMG-
 233 CoA leading to a subsequent decrease in its levels. This substrate-enzyme
 234 reaction leads to increases in geranyl-PP, farnesyl-PP, bound farnesyl-PP
 235 with squalene synthase, squalene, lanosterol and finally cholesterol. The ob-
 236 served decrease in each entity within the network at approximately 20 hours
 237 is the result of global and local feedbacks within the system. Firstly, the in-
 238 crease in cholesterol leads, via the negative feedback between cholesterol and
 239 SREBP-2 transcription of HMGCR mRNA and squalene synthase mRNA,
 240 to a decrease in the concentration of HMGCR and squalene synthase, re-
 241 spectively. This globally controlled feedback reduction in the two enzymes
 242 subsequently means less of the central cascade products are now being synthe-
 243 sised. This feedback is explored in more detail in Section 7.1. Simultaneously,

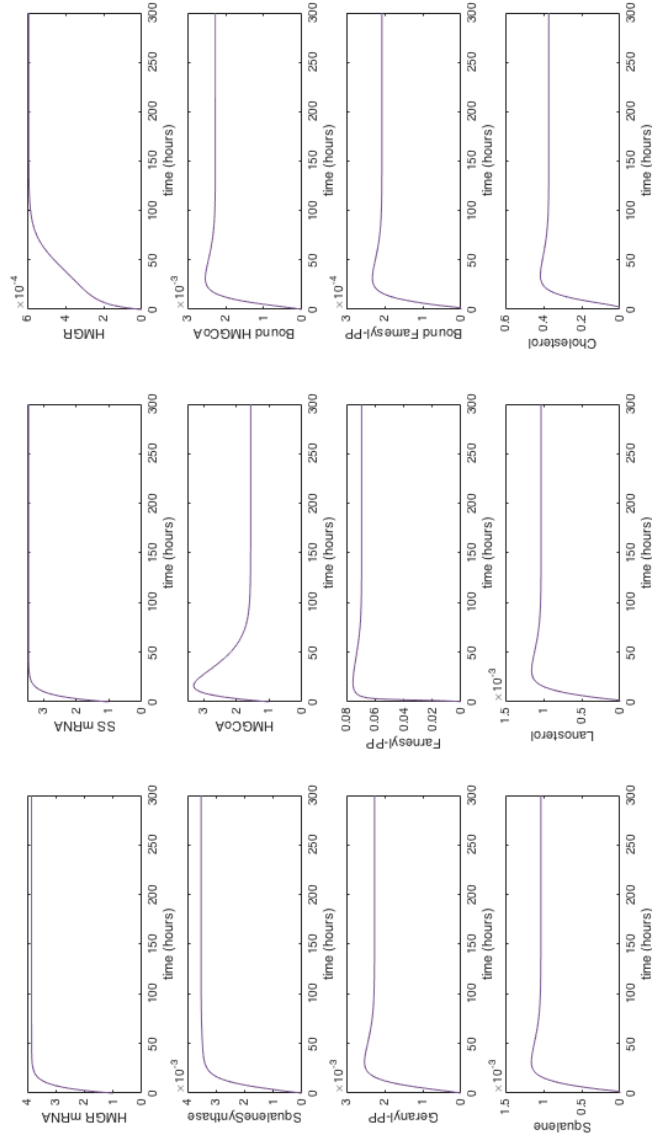


Figure 2: Numerical solutions to equations (34) to (46) with parameter values detailed in Table 2. Solutions show the response of HMGCR and squalene synthase mRNA to initial zero cholesterol concentrations, the subsequent increase in HMGCR and squalene synthase which allows the synthesis of cascade products geranyl-PP, farnesyl-PP, squalene, lanosterol and finally cholesterol.

244 and more locally, negative feedbacks from geranyl-PP, farnesyl-PP, lanosterol
245 and cholesterol seek to limit the enzymatic action of HMGCR and squalene
246 synthase by increasing their rates of degradation. These local feedbacks are
247 explored in more detail in Section 9.

248 The subsequent decrease in cholesterol levels leads to a small increase in
249 HMGCR and squalene synthase mRNA transcription. Eventually the so-
250 lutions evolve to reach a steady-state. Solutions of the model show that
251 concentrations of both farnesyl-PP and cholesterol are greater than those of
252 other cascade products; geranyl-PP, squalene and lanosterol. One reason for
253 this could be because farnesyl-PP is a major branch point in the pathway
254 and is used (as is cholesterol) in a greater number of cell processes, thus their
255 respective concentrations need to be higher. We note that HMGCoA initially
256 increases (as a result of its own synthesis) before decreasing to steady-state
257 levels due to increased HMGCR levels.

258 Direct comparison with experimental values for the concentration of each en-
259 tity within the pathway is difficult given a lack of reported values in the lit-
260 erature. In the case of HMGCR mRNA we can approximate this via Rudling
261 et al. [30] who states there are 30 copies of HMGCR mRNA found in each
262 human liver cell under basal conditions. This leads to a concentration of
263 3.00×10^{10} molecules/ml, for which our result of 1.13×10^{10} molecules/ml is
264 very similar. Our concentrations of HMGCR mRNA, HMGCR and cholest-
265 terol are also in agreement with those previously reported in Bhattacharya
266 et al. [2].

267 5. Model Analysis

268 In this and subsequent sections we undertake a comprehensive analysis of the
269 mevalonate pathway model. Given the overall network complexity and diffi-
270 culty in obtaining analytical solutions to the system of governing equations
271 we begin with a sensitivity analysis in Section 5.1. Results from this high-
272 light enzyme-rate rate limiting steps within the pathway which are explored
273 in more detail analytically in Section 6. We consider a simplified model of
274 the pathway, containing the key enzyme-substrate reactions and feedbacks
275 within the pathway in Section 7, in order to examine the steady-states of the
276 system and their stability. Numerical experiments are conducted in Section 8
277 to verify our findings.

278 *5.1. Sensitivity analysis*

279 We conducted a local sensitivity analysis, varying each parameter in turn, up
280 to 100-fold above and below the values reported in Table 2. We quantitatively
281 measured, primarily, the effect of parameter variation on the steady-state
282 cholesterol concentrations (in relation to the unperturbed system) whilst also
283 looking for significant variations in key elements of the pathway, for exam-
284 ple steady-state farnesyl-PP concentrations and differences in the dynamic
285 behaviour of each model variable. Varying the model parameters up to 100-
286 fold allows us to explore the robustness of the pathway to changes greater
287 than those biologically feasible thereby ensuring all possible effects have been
288 explored.

289 In what follows we present our results by discussing parameters related to
290 specific processes within the pathway (e.g. HMGCR synthesis) wherever pos-
291 sible. Given their number and to ascertain their effects separately, negative
292 feedbacks within the pathway are discussed separately in Sections 7.1 and 9.
293 Not all parameters caused a notable change in the system; only those that
294 did are discussed here.

The results of our local sensitivity analysis were subsequently confirmed by
a metabolic control analysis in which the relationship between the system
steady-states and the properties of the individual reactions was explored.
The response coefficients were calculated via

$$\mathbf{R} = R_m^i = \frac{P_m}{S_i^{st}} \frac{\partial S_i^{st}}{\partial P_m},$$

295 where \mathbf{R} is the matrix of response coefficients, P_m is each parameter value
296 and S_i^{st} is the corresponding metabolite (mRNA/substrate/enzyme in our
297 system) at steady-state.

298 *5.1.1. HMGCoA synthesis (ω)*

299 The HMGCoA-HMGCR reaction point in the pathway is the first rate lim-
300 iting step in the cascade [34] and HMGCoA is the starting point of all the
301 central cascade reactions. Hence decreasing HMGCoA availability 10-fold
302 leads to an abundance of enzyme HMGCR (over 300% more) and leads to
303 a reduction of over 90% in all cascade products except farnesyl-PP (73%).

304 Increasing the rate of HMGCoA synthesis 10-fold, decreases HMGCR con-
305 centrations by almost 100% due to the abundance of HMGCoA, but has only
306 a moderate effect on the concentrations of cascade products (around 33%)
307 including cholesterol. In all cases farnesyl-PP is more tightly regulated, and
308 exhibits a smaller percentage change, than the rest of the cascade products.
309 Thus the farnesyl-PP squalene synthase substrate-enzyme reaction appears
310 to act as a second rate limiting step in the pathway, lending greater control
311 to downstream cholesterol concentrations. This is explored in further detail
312 in Section 6.

313 5.1.2. Genetic regulation of HMGCR (μ_1 , μ_3 , δ_1 and δ_3)

314 Parameter changes that induce an increase in HMGCR mRNA or HMGCR
315 did not greatly affect the pathway. This is because the substrate HMGCoA is
316 almost completely utilised and thus cholesterol increases are limited in spite
317 of the amount of HMGCR being produced i.e. the binding of HMGCoA
318 and HMGCR has reached its upper limit. This combined with the results of
319 altering the rate of HMGCoA synthesis ω , show there is a careful balance of
320 both enzyme HMGCR and substrate HMGCoA in order for cholesterol to be
321 produced. If there is an abundance of either enzyme or substrate, the reaction
322 will be limited by the lower of the two concentrations without a significant
323 effect on cholesterol concentrations. However, biologically, we would always
324 expect the concentration of enzyme to be less than the concentration of
325 substrate.

326 On the other hand, decreasing the rates of transcription and translation (μ_1 ,
327 μ_3) or increasing the rates of HMGCR mRNA and HMGCR degradation (δ_1
328 and δ_3) has a significant effect on cholesterol concentrations, as well as de-
329 creasing all the other cascade products. For example, decreasing the value of
330 μ_1 or μ_3 by even one order of magnitude causes an 88% decrease in cholesterol
331 levels. Increasing the value of δ_1 or δ_3 by one order of magnitude has a simi-
332 lar effect. Concentrations of HMGCR are, unsurprisingly, decreased leading
333 to an accumulation of HMGCoA. Products of the central cascade are all
334 decreased by around 88% (farnesyl-PP 68%). The reduction of cholesterol
335 upregulates squalene synthase via the local squalene synthase degradation
336 feedback shown in Figure 1.

337 *5.2. Genetic regulation of squalene synthase (μ_2 , μ_4 , δ_2 and δ_4)*

338 Parameter changes that cause an increase in squalene synthase mRNA or
339 squalene synthase do not greatly affect the pathway. An abundance in squalene
340 synthase leads to a significant decrease in farnesyl-PP, but the increase
341 in cholesterol concentrations (as well as those of squalene and lanosterol) is
342 only around 7%. Increasing the amount of squalene synthase does have a
343 greater effect on cholesterol concentrations than increasing the amount of
344 HMGCR, however we again see the balance of enzyme and substrate limiting
345 the reaction.

346 Parameter changes that cause a decrease in squalene synthase mRNA or
347 squalene synthase have less of an effect on concentrations of cholesterol than
348 a decrease in HMGCR. For example, decreasing the value of transcription of
349 squalene synthase mRNA (μ_2) or translation of squalene (μ_4), by one order of
350 magnitude causes a 39% decrease in cholesterol levels. Increasing the value of
351 δ_2 (the degradation rate of squalene synthase mRNA) or δ_4 (the degradation
352 rate of squalene synthase) by one order of magnitude has the same effect. In
353 each case concentrations of squalene synthase are, unsurprisingly, decreased
354 which leads to an accumulation of farnesyl-PP. Products downstream of the
355 farnesyl-PP-squalene synthase reaction (bound farnesyl-PP, squalene, lanosterol
356 and cholesterol) are all decreased by around 39%, another indicator of
357 a limiting step at this point in the pathway. This decline in cholesterol and
358 other cascade product concentrations slightly reduces HMGCR degradation
359 (2% change) as expected. We can demonstrate the effect of the HMGCR
360 degradation feedbacks by comparing the concentrations between one and
361 two orders of magnitude change in δ_2 and δ_4 , where cholesterol and lanosterol
362 concentrations decrease by 92.6%, HMGCR concentrations increase by
363 8%.

364 *5.2.1. Association and disassociation of HMGCR for HMGCoA and farnesyl-PP for squalene (κ_4 , κ_{-4} , κ_5 and κ_{-5})*

366 Altering the association rates of each of these enzyme and substrate reactions
367 has a small effect on cholesterol levels and downstream cascade products.
368 We found that decreasing the rate of binding (κ_5) in the squalene synthase-
369 farnesyl-PP reaction, has a greater effect on cholesterol and downstream
370 cascade product levels than decreasing the binding rate (κ_4) in the HMGCR-
371 HMGCoA reaction, again indicating the importance of the squalene synthase-

372 farnesyl-PP rate limiting step. Altering the disassociation rates (κ_{-4} and
373 κ_{-5}) of each reaction has no effect on cholesterol levels or indeed the rest of
374 the system.

375 *5.2.2. Production of geranyl-PP and squalene (μ_5 and μ_7)*

376 Decreasing the rate at which either of the enzyme-substrate complexes are
377 converted to a product decreases the concentrations of the respective down-
378 stream products. Specifically decreasing the rate of squalene production, has
379 a lesser effect on products downstream of the reaction than decreasing the
380 rate at which geranyl-PP is produced. Decreasing either of these rates leads
381 to an increase in both substrate concentrations but, counter-intuitively, de-
382 creases the concentration of both enzymes. This happens for two reasons;
383 firstly the enzymes are held in their bound rather than free forms (shown by
384 an increase in bound substrate concentrations). Secondly, increases in each
385 substrate concentration ensures that any enzyme synthesised or returned
386 from disassociation with the enzyme-substrate complex is quickly bound by
387 the excess substrate. Increasing the rate of complex to product conversion
388 (μ_5 and μ_7) has very little effect on downstream cascade products, given they
389 are limited by the amount of available substrate (HMGCoA and farnesyl-PP,
390 respectively).

391 *5.2.3. Production of farnesyl-PP and lanosterol (μ_6 and μ_8)*

392 Increasing the production rate of farnesyl-PP and lanosterol has very little
393 effect on the pathway and cholesterol levels. Interestingly, decreasing the
394 production rate of farnesyl-PP has a greater effect on the central cascade
395 products than decreasing the production of lanosterol. Decreasing μ_6 100-
396 fold reduces cholesterol concentrations by 22%, reducing the degradation of
397 HMGCR and squalene synthase, which increase by 1.5% and 3.4% respec-
398 tively.

399 *5.2.4. Production of cholesterol (μ_9)*

400 Increasing the rate of production of cholesterol does not greatly affect choles-
401 terol concentrations, however decreasing μ_9 has a small to moderate effect
402 on cholesterol levels. However, the changes in lanosterol concentrations as
403 a result, have the greatest effect on HMGCR concentrations via the local

404 degradation feedbacks, in comparison to parameter changes that induce an
405 increase or reduction of geranyl-PP or farnesyl-PP - the other degradation
406 feedbacks on HMGCR.

407 *5.2.5. Degradation of farnesyl-PP (δ_6)*

408 Decreasing the degradation rate of farnesyl-PP slightly increases the steady-
409 state concentration of cholesterol and other downstream cascade products
410 (within 10%). As expected this negatively effects both HMGCR and squalene
411 synthase via the degradation feedbacks by a moderate amount in order to
412 limit the increase in farnesyl-PP and cholesterol. However, increasing the
413 degradation rate of farnesyl-PP by just one order of magnitude impacts the
414 downstream cascade significantly, decreasing the concentrations of squalene,
415 lanosterol and cholesterol by 52.4% (33.6% for farnesyl-PP). The decrease in
416 cholesterol subsequently up-regulates HMGCR and squalene synthase levels.
417 Interestingly, squalene synthase is increased slightly more than HMGCR.
418 This could be to counteract the loss of farnesyl-PP through degradation, to
419 ensure cholesterol concentrations are maintained.

420 *5.2.6. Degradation of geranyl-PP and lanosterol (δ_5 and δ_7)*

421 Altering the degradation rates of geranyl-PP and lanosterol have very little
422 effect on the pathway or steady-state cholesterol levels. Increasing degra-
423 dation of geranyl-PP by 100 fold moderately reduces the concentrations of
424 the central cascade and slightly upregulates squalene synthase and HMGCR.
425 Squalene synthase more so. Increasing the degradation rate of lanosterol by
426 100-fold also reduces the concentrations of lanosterol and cholesterol by ap-
427 proximately the same amount, however, HMGCR is upregulated more than
428 squalene synthase. This is a result of the change in central cascade products
429 and the role of the Michaelis-Menten responses affecting the feedbacks to
430 HMGCR and squalene synthase, respectively.

431 *5.2.7. Cholesterol degradation (δ_8)*

432 Varying the rate of cholesterol degradation greatly effects cholesterol con-
433 centrations. As expected the increase in cholesterol concentrations downreg-
434 ulates HMGCR and squalene synthase via the local degradation feedbacks,

435 however only by around 1%. Similarly for decreased cholesterol concentra-
436 tions, HMGCR and squalene synthase are upregulated by around 0.1%.

437 *5.2.8. Genetic binding affinities and stoichiometric coefficients (κ_1 , κ_2 , κ_3 ,*
438 *x_c , x_h and x_s)*

439 Binding affinities and stoichiometric coefficients involved with the genetic
440 regulation of HMGCR and squalene synthase have very little effect on the
441 system. Interestingly, reducing parameters involved in genetic regulation of
442 HMGCR has a greater effect on the system than those in regulating squalene
443 synthase, however these changes would indicate a fraction of a binding site
444 which is biologically infeasible. Furthermore, decreasing the value of κ_3 , the
445 regulation of HMGCR and squalene synthase by cholesterol has the effect
446 of decreasing cholesterol concentrations, significantly for a 100-fold decrease,
447 whilst slightly upregulating HMGCR and squalene synthase.

448 *5.2.9. Sensitivity analysis summary*

449 Local sensitivity analysis has highlighted that a decrease in HMGCR (the
450 first rate limiting step in the pathway), caused by parameters linked with
451 its genetic regulation, significantly decreases steady-state cholesterol concen-
452 trations. However, increases in products linked with genetic regulation of
453 HMGCR do not have a significant impact on steady-state cholesterol concen-
454 trations, due to the occurrence of the second rate limiting step between
455 squalene synthase and farnesyl-PP. The effect of decreasing products linked
456 with genetic regulation of squalene synthase is not as significant as those
457 linked with regulation of HMGCR.

458 An increase in products prior to the reaction of farnesyl-PP with squalene
459 synthase rarely causes a significant change in cholesterol levels (the excep-
460 tion being a decrease in μ_5 reducing cholesterol concentrations significantly),
461 whilst the degradation of farnesyl-PP has a high effect on downstream prod-
462 uct concentrations. We found that, with the exception of decreasing μ_5 , the
463 rates of geranyl-PP and squalene formation, from the two enzyme-substrate
464 reactions within the pathway, have a moderate effect on limiting downstream
465 products formed in the pathway. In contrast, altering the rates of geranyl-
466 PP and lanosterol degradation have little impact on the pathway. Cellular
467 cholesterol concentrations are very sensitive to changes in the rate of chole-

468 terol esterification (degradation) without much interruption to the rest of the
 469 pathway.

470 Our results, as summarised in Table 3, demonstrate that the two rate limiting
 471 steps of HMGCR and HMGC_oA and farnesyl-PP and squalene synthase,
 472 coupled with the negative feedback between cholesterol and SREBP-2, act
 473 as core regulators of products within the central cascade. The HMGC_oA
 474 and HMGCR rate limiting step is aimed at controlling production of central
 475 cascade substrates, whilst that of farnesyl and squalene synthase appears
 476 two-fold; it acts to control the levels of lanosterol and ultimately cholesterol
 477 produced, but also regulate those of farnesyl-PP, given its role in other cell
 478 signalling pathways. Whilst the enzyme rate limiting step of HMGCR and
 479 HMGC_oA follows one-to-one stoichiometry, this differs for squalene synthase
 480 and farnesyl-PP; two molecules of farnesyl-PP reversibly bind to squalene
 481 synthase, to produce one molecule of complex bound farnesyl-PP. The effect
 482 of this is investigated further in Section 6.

Table 3: Sensitivity analysis summary. Results here indicate up to a 10% (denoted ‘+’ or ‘-’), 10-50% (‘++/- -’), greater than 50% (‘+++/- -’) variation or no change (‘NC’) in the steady-state cholesterol levels for the parameterisation detailed in Table 1 for 10-fold parameter variations.

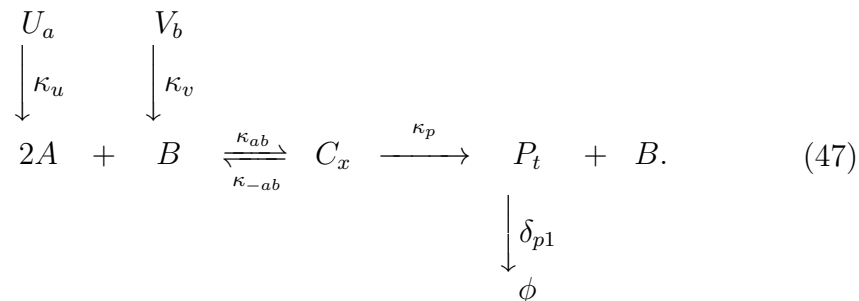
Change Made	Parameters Involved	Effect on Cholesterol
Increased HMGC _o A	ω	++
Decreased HMGC _o A	ω	—
Increased HMGCR	$\mu_1, \mu_3, \delta_1, \delta_3$	NC
Decreased HMGCR	$\mu_1, \mu_3, \delta_1, \delta_3$	- - -
Increased Squalene synthase	$\mu_2, \mu_4, \delta_2, \delta_4$	+
Decreased Squalene Synthase	$\mu_2, \mu_4, \delta_2, \delta_4$	- -
Increased Association of Enzymes	κ_4, κ_5	+
Decreased Association of Enzymes	κ_4, κ_5	- -
Dissociation of Enzymes	κ_{-4}, κ_{-5}	NC
Increased Product formation	μ_5, μ_7	NC
Decreased Product formation	μ_5	- - -
Decreased Product formation	μ_7	- -
Increased degrataion of FPP	δ_6	- - -
Decreased degradation of FPP	δ_6	+
Increased degradation	δ_5, δ_7	-
Decreased degradation	δ_5, δ_7	NC
Degradation of cholesterol	δ_8	+ + + / - - -
Stoichiometric coefficients	x_c, x_h, x_s	NC
Genetic binding affinities	K_1, K_2	NC
Increased genetic binding affinity	K_3	NC

Table 3 – continued

Decreased genetic binding affinity	K_3	-
Half Max degradation binding	$K_6, K_7, K_8, K_9, K_{10}$	NC
Increased Product formation	μ_6, μ_8	NC
Decreased Product formation	μ_6	-
Decreased Product formation	μ_8	NC
Increased Product formation	μ_9	NC
Decreased Product formation	μ_9	-

483 6. The farnesyl-PP - squalene synthase rate limiting step

484 Sensitivity analysis of the previous section has revealed evidence of two rate
 485 limiting steps working together to regulate homeostatic cholesterol levels.
 486 The first is that of the well documented HMGCR HMGCoA reaction, whilst
 487 the second involves farnesyl-PP reacting with squalene synthase. Here we
 488 investigate the role of the latter reaction, in particular the role of the stoi-
 489 chometry between farnesyl-PP and squalene synthase in effecting the creation
 490 of products downstream of this reaction. In order to do so we consider a sim-
 491 plified version of this part of the network as given by the reaction stated in
 492 equation (47).



493 In this case we have employed A to represent farnesyl-PP, B squalene syn-
 494 thase, C_x the enzyme-substrate complex, P_t squalene and U_a and V_b the influx
 495 of substrate and enzyme respectively. For simplicity we assume a constant
 496 source of enzyme U_a and substrate V_b , at rates κ_u and κ_v , respectively, and we
 497 have removed the effect of the feedback of cholesterol onto squalene synthase
 498 degradation. Here κ_{ab} and κ_{-ab} represent the binding and unbinding, respec-
 499 tively, of A and B , κ_p is the rate at which the product is formed and finally

500 the degradation of P is represented by δ_{p1} . We observe that $A, B, C_x, P_t \geq 0$
 501 is required for biologically feasible solutions.

502 Applying the law of mass action to equation (47) leads to

$$\frac{da}{dt} = -2a^2b\kappa_{ab} + 2c_x\kappa_{-ab} + u_a\kappa_u, \quad (48)$$

$$\frac{db}{dt} = -a^2b\kappa_{ab} + c_x\kappa_{-ab} + v_b\kappa_v + c_x\kappa_p, \quad (49)$$

$$\frac{dc_x}{dt} = a^2b\kappa_{ab} - c_x\kappa_{-ab} - c_x\kappa_p, \quad (50)$$

$$\frac{dp_t}{dt} = c_x\kappa_p - p_t\delta_{p1}, \quad (51)$$

503 with the initial conditions

$$a(0) = a_0, \quad b(0) = b_0, \quad c_x(0) = 0, \quad p_t(0) = 0.$$

We observe that the addition of equations (49) and (50) leads to

$$\frac{da}{dt} + \frac{db}{dt} = v_b\kappa_v,$$

504 which for large time becomes

$$b + c_x \sim v_b\kappa_v t. \quad (52)$$

505 This suggests that a, b, c_x and subsequently p_t follow solutions of the form

$$a \sim a_0 t^\alpha, \quad b \sim b_0 t^\beta, \quad c_x \sim c_{x0} t^\gamma \quad \text{and} \quad p_t \sim p_{t0} t^\lambda. \quad (53)$$

506 Substitution of these solution approximations into equations (48)-(51) leads
 507 to

$$a \sim Kt^{-1/2}, \quad b \sim v_b\kappa_p t, \quad c_x \sim \frac{u_a\kappa_u}{2\kappa_p} \quad \text{and} \quad p_t \sim \frac{u_a\kappa_u}{2\delta_{p1}}. \quad (54)$$

508 for which we have the results $a \rightarrow 0, b \rightarrow \infty$ for finite c_x and p_t . This
 509 result demonstrates that the substrate farnesyl-PP tends to zero, squalene
 510 synthase grows unboundedly in time whilst the complex (bound farnesyl-PP)
 511 and product (squalene) remain bounded for any degree of influx.

512 From this analysis we can conclude that the rate limiting interaction of squalene synthase and farnesyl-PP would ensure product formation (squalene) is
513 finite and bounded regardless of whether the substrate (farnesyl-PP) or enzyme (squalene synthase) concentrations are bounded. Furthermore, if the
514 levels of squalene are bounded the subsequent products i.e. lanosterol and cholesterol will also be bounded. Thus the mechanism has the downstream
515 effect of ensuring cholesterol levels do not become excessive and alleviates the likelihood of biosynthetic cytotoxicity.
516
517
518
519

520 7. Steady-state stability analysis

521 The recent work of Bhattacharya et al. [2] demonstrated that a nonlinear ODE model describing cholesterol biosynthesis via HMGCR mRNA trans-
522 cription and subsequent HMGCR translation was monostable. The mevalonate pathway examined here is essentially an extension of that model which
523 incorporates further pathway details between HMGCR and cholesterol synthesis. The increased complexity raises the question as to whether the system
524 exhibits a single real stable steady-state. In this section we utilise a reduction of the full model derived in Section 3 to investigate this.
525
526
527
528

529 7.1. Model reduction

530 Given the complexity of the governing equations of the full pathway model system (equations (34)-(45)) we begin by simplifying the full pathway (hence-
531 forth known as the full model) of Figure 1 by that shown in Figure 3. Here the core product forming and branching points in the pathway have been
532 retained such that w represents SREBP-2, u HMGCR, v squalene synthase, x HMGCoA, y farnesyl-PP and z cholesterol. Here x is produced at a rate
533 A and the negative feedbacks between each relevant component have been included. We further assume that the cholesterol-SREBP-2 negative feed-
534 back is the fastest acting process in this reduced network, followed by the synthesis of HMGCR and squalene synthase, which occurs an order of mag-
535 nitude slower. Subsequently the formation of x , y and z are assumed to be the slowest in the pathway. Finally, x , y and z decay proportional to their
536
537
538
539
540
541
542

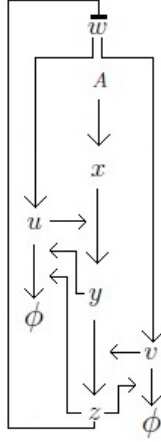


Figure 3: A model reduction of the mevalonate pathway which incorporates the key enzyme and substrate synthesis processes and branch points, along with their respective feedbacks. Here w represents SREBP-2, u HMGCR, v squalene synthase, x HMGCoA, y farnesyl-PP and z cholesterol, where x is produced at a rate A . It is assumed, as with the full-pathway model, that x , y and z decay proportional to their respective concentrations (not shown here).

543 Applying these assumptions and the law of mass action to the reduced path-
 544 way of Figure 3 leads to the following non-dimensional system of equations

$$\dot{x} = A - \mu_{r1}xu - \delta_{r1}x, \quad (55)$$

$$\dot{y} = \mu_{r1}\beta_x xu - \mu_{r2}yv - \delta_{r2}y, \quad (56)$$

$$\dot{z} = \mu_{r2}\beta_y yv - \delta_{r3}z, \quad (57)$$

$$\epsilon \dot{u} = \mu_{r3}w - \delta_{r4}u \left(\delta_{uz} \frac{z}{\kappa_{r1} + z} + \delta_{uy} \frac{y}{\kappa_{r2} + y} + 1 \right), \quad (58)$$

$$\epsilon \dot{v} = \mu_{r4}w - \delta_{r5}v \left(\delta_{vz} \frac{z}{\kappa_{r3} + z} + 1 \right), \quad (59)$$

$$\epsilon^2 \dot{w} = \frac{\alpha_{r1}}{\kappa_{r4} + z^{n1}} - \delta_{r6}w, \quad (60)$$

545 with the initial conditions

$$x = 1, \quad y = 1, \quad z = 1, \quad u = 1, \quad v = 1 \quad \text{and} \quad w = 1. \quad (61)$$

546 Here ϵ represents a small parameter and the remaining model parameters are
 547 given by μ_{r1} which represents the rate at which x produces y , μ_{r2} is the rate
 548 at which y produces z , μ_{r3} the rate at which u is transcribed, μ_{r4} the rate

549 at which v is transcribed, β_x and β_y are non-dimensional ratios representing
550 the initial dimensional concentrations of x and y , and y and z , respectively
551 and α_{r1} that rate at which w is produced. The effective binding sites of
552 cholesterol on SREBP-2 is represented by n_1 and $\delta_{r1,2,3,4,5,6}$ represent the
553 rate of degradation of x, y, z, u, v and w , respectively. Finally, $\kappa_{r1,2,3,4}$ are the
554 Michaelis-Menten constants associated with the feedback of z on the rate
555 of u degradation, y on that of u degradation, z on v degradation and z on
556 w inhibition, respectively and δ_{uz} , δ_{uy} and δ_{vz} are dimensionless constants
557 respectively representing their effect. As with the full model of Section 3
558 and for the sake of simplicity we henceforth assume, unless otherwise stated,
559 $\delta_{uz} = 1 = \delta_{uy} = \delta_{vz}$.

560 Taking the $O(1)$ expansion of equations (55)-(60) leads to

$$\dot{x} = A - \frac{\tilde{\mu}_{r1}x}{(\kappa_{r4} + z^{n_1}) \left(\frac{z}{\kappa_{r1}+z} + \frac{y}{\kappa_{r2}+y} + 1 \right)} - \delta_{r1}x, \quad (62)$$

$$\dot{y} = \frac{\tilde{\mu}_{r1}\beta_x x}{(\kappa_{r4} + z^{n_1}) \left(\frac{z}{\kappa_{r1}+z} + \frac{y}{\kappa_{r2}+y} + 1 \right)} - \frac{\tilde{\mu}_{r2}y}{(\kappa_{r4} + z^{n_1}) \left(\frac{z}{\kappa_{r3}+z} + 1 \right)} - \delta_{r2}y, \quad (63)$$

$$\dot{z} = \frac{\mu_{r2}\beta_y y}{(\kappa_{r4} + z^{n_1}) \left(\frac{z}{\kappa_{r3}+z} + 1 \right)} - \delta_{r3}z, \quad (64)$$

561 where

$$\tilde{\mu}_{r1} = \frac{\mu_{r1}\mu_{r3}\alpha_{r1}}{\delta_{r4}\delta_{r6}} \quad \text{and} \quad \tilde{\mu}_{r2} = \frac{\mu_{r2}\mu_{r4}\alpha_{r1}}{\delta_{r5}\delta_{r6}}. \quad (65)$$

562 Assuming the concentrations of cholesterol and farnesyl-PP are in excess
563 and the rates of affinity of cholesterol for HMGCR and squalene synthase
564 (k_{r1} and k_{r3}) and farnesyl-PP for HMGCR are significantly high such that
565 $k_{r1}, k_{r3} \ll z$ and $k_{r2} \ll y$ leads to $k_{r1} + z \sim z$, $k_{r2} + y \sim y$ and $k_{r3} + z \sim z$.
566 Thus

$$\dot{x} = A - \frac{\mu_{rr1}x}{\kappa_{r4} + z^{n_1}} - \delta_{r1}x = f(x, y, z), \quad (66)$$

$$\dot{y} = \frac{\mu_{rr1}\beta_x x}{\kappa_{r4} + z^{n_1}} - \frac{\mu_{rr2}y}{\kappa_{r4} + z^{n_1}} - \delta_{r2}y = g(x, y, z), \quad (67)$$

$$\dot{z} = \frac{\mu_{rr2}\beta_y y}{\kappa_{r4} + z^{n_1}} - \delta_{r3}z = h(x, y, z), \quad (68)$$

567 where $\mu_{rr1} = \frac{1}{3}\tilde{\mu}_{r1}$ and $\mu_{rr2} = \frac{1}{2}\tilde{\mu}_{r2}$.

568 *7.2. Steady-state stability*

Solving for the steady-states (x^*, y^*, z^*) of equations (66)-(68) leads to the polynomial (recalling that n_1 is an integer)

$$z^{2n_1+1}(\delta_{r1}\delta_{r2}\delta_{r3}) + z^{n_1+1}(\delta_{r1}\delta_{r3}\mu_{rr2} + 2\delta_{r1}\delta_{r2}\delta_{r3}\kappa_{r4} + \delta_{r2}\delta_{r3}\mu_{rr1}) + z(\delta_{r2}\delta_{r3}\mu_{rr1}\kappa_{r4} + \delta_{r1}\delta_{r2}\delta_{r3}\kappa_{r4}^2 + \delta_{r1}\delta_{r3}\mu_{rr2}\kappa_{r4} + \delta_{r3}\mu_{rr1}\mu_{rr2}) - A\mu_{rr1}\mu_{rr2}\beta_x\beta_y = 0, \quad (69)$$

569 which via Descartes' rule of signs [27] has only one positive root z^* . From
570 (66) and (67) it follows that the corresponding x^* and y^* are also positive.

571 Now the Jacobian of equations (66)-(68) is given by

$$J = \begin{pmatrix} \frac{-\mu_{rr1}}{\kappa_{r4}+z^{n_1}} - \delta_{r1} & 0 & \frac{n_1\mu_{rr1}xz^{n_1-1}}{(\kappa_{r4}+z^{n_1})^2} \\ \frac{\mu_{rr1}\beta_x}{\kappa_{r4}+z^{n_1}} & \frac{-\mu_{rr2}}{\kappa_{r4}+z^{n_1}} - \delta_{r2} & \frac{-n_1\mu_{rr1}\beta_xxz^{n_1-1}}{(\kappa_{r4}+z^{n_1})^2} + \frac{n_1\mu_{rr2}yz^{n_1-1}}{(\kappa_{r4}+z^{n_1})^2} \\ 0 & \frac{\mu_{rr2}\beta_y}{\kappa_{r4}+z^{n_1}} & \frac{-n_1\mu_{rr2}\beta_yyz^{n_1-1}}{(\kappa_{r4}+z^{n_1})^2} - \delta_{r3} \end{pmatrix},$$

572 which allows us to determine the characteristic equation

$$\lambda^3 + a_1\lambda^2 + a_2\lambda + a_3 = 0,$$

573 where

$$a_1 = -(f_x + g_y + h_z), \quad a_2 = f_x(g_y + h_z) + g_y h_z - g_z h_y \\ \text{and} \quad a_3 = -(f_x(g_y h_z - g_z h_y) + f_z g_x h_y). \quad (70)$$

574 Now for (x^*, y^*, z^*) to be stable we require $Re(\lambda) < 0$ meaning that the
575 following Routh–Hurwitz conditions [27] must hold

$$a_1 > 0, \quad a_3 > 0 \quad \text{and} \quad a_1 a_2 - a_3 > 0. \quad (71)$$

576 It is easily seen that $f_x, g_y, h_z < 0$ (diagonal entries of J) whilst $f_z, g_x, h_y > 0$.
577 The remaining non-zero term of the Jacobian is

$$g_z = - \left(\frac{n_1 z^{n_1-1}}{\kappa_{r4} + z^{n_1}} \right) \left(\frac{\mu_{rr1}\beta_x x}{\kappa_{r4} + z^{n_1}} - \frac{\mu_{rr2}y}{\kappa_{r4} + z^{n_1}} \right).$$

578 Both sets of brackets are clearly positive at steady-state (the second set from
579 (67)) and so we have $g_z < 0$ at the steady-state.

580 Using the signs of the Jacobian entries at steady state immediately gives
581 $a_1 > 0$ and, with a little work we can readily use them to deduce that
582 $a_1 a_2 - a_3 > 0$. In order to show the remaining required inequality we cannot
583 use the signs of the Jacobian entries alone. Instead we first simplify notation
584 by writing

$$\alpha_1 = \frac{-\mu_{rr1}}{\kappa_{r4} + z^{n_1}}, \quad \alpha_2 = \frac{-\mu_{rr2}}{\kappa_{r4} + z^{n_1}},$$

$$\gamma_1 = \frac{n_1 \mu_{rr1} x z^{n_1-1}}{(\kappa_{r4} + z^{n_1})^2}, \quad \gamma_2 = \frac{n_1 \mu_{rr2} y z^{n_1-1}}{(\kappa_{r4} + z^{n_1})^2},$$

585 noting that each of these is non-negative. The Jacobian can then be written
586 as

$$J = \begin{pmatrix} -\alpha_1 - \delta_{r1} & 0 & \gamma_1 \\ \alpha_1 \beta_x & -\alpha_2 - \delta_{r2} & -\gamma_1 \beta_x + \gamma_2 \\ 0 & \alpha_2 \beta_y & -\gamma_2 \beta_y - \delta_{r3} \end{pmatrix},$$

587 and a_3 as

$$\begin{aligned} a_3 &= (\alpha_1 + \delta_{r1}) ((\alpha_2 + \delta_{r2})(\gamma_2 \beta_y + \delta_{r3}) + \alpha_2 \beta_y (\gamma_1 \beta_x (\gamma_1 \beta_x - \gamma_2)) \\ &\quad - \gamma_1 \alpha_1 \beta_x \alpha_2 \beta_y) \\ &= (\alpha_1 + \delta_{r1}) (\alpha_2 \delta_{r3} + \gamma_2 \beta_y \delta_{r2} + \delta_{r2} \delta_{r3}) + \delta_{r1} \alpha_2 \gamma_1 \beta_x \beta_y. \end{aligned}$$

588 Since each symbol is non-negative we immediately have that $a_3 > 0$ as re-
589 quired. Thus (x^*, y^*, z^*) is stable.

590 In order to provide a check of the stability obtained from the reduced model,
591 we numerically calculated the Jacobian for the full model system using the
592 parameter values detailed in Table 2. All eigenvalues are found to be negative
593 or approximately zero, for a range of initial conditions.

594 8. Periodic solutions

595 The results of Section 7 have demonstrated that the mevalonate pathway
596 exhibits one real steady-state. Both this model and that of Bhattacharya et

597 al. [2] include the negative regulation of SREBP-2 by cholesterol. In the case
598 of the three variable model analysed by Bhattacharya and colleagues, they
599 demonstrated that the system could exhibit periodic behaviour under certain
600 model parameterisations. As such we now investigate numerically whether it
601 is possible for the mevalonate pathway model to exhibit oscillatory solutions.

602 Our investigations focused on the parameters κ_1 , κ_3 , x_c and δ_8 given they
603 are directly involved in the cholesterol-SREBP-2 feedback, are parameters
604 for which periodic behaviour was shown in [2], and the results of varying all
605 other model parameters in Section 5.1 produced no periodic behaviour.

606 Local sensitivity analysis of κ_1 , κ_2 , κ_3 , x_c and δ_8 revealed the presence of
607 periodic (damped or undamped) behaviour within the system, an example
608 of which is shown in Figure 4. The presence of oscillatory behaviour for
609 other parameter values showed comparable results. We note the increase in
610 concentration of HMGCoA in Figure 4 is a result of the choice in w made to
611 demonstrate the existence of oscillatory solutions. We sought to numerically
612 investigate further the likelihood of a Hopf bifurcation within the mevalonate
613 pathway, as a result of this feedback, and undertook a phase space analysis
614 using MATLAB'S ode15s solver and the plot3 function. We found that the
615 system exhibits an unstable fixed point surrounded by a stable limit cycle
616 and thus appears to undergo a supercritical Hopf bifurcation (results not
617 shown). This was found to be the case when considering the HMGCR mRNA,
618 HMGCR and cholesterol phase space as well as that for squalene synthase
619 mRNA, squalene and cholesterol.

620 These results indicate that the full mevalonate pathway model is able to pro-
621 duce periodic behaviour, similar to that related to more simplified networks
622 within it (e.g. HMGCR mRNA, HMGCR and cholesterol), so long as the
623 global scale negative feedback between cholesterol and SREBP-2 is present.

624 **9. Investigating feedbacks**

625 In this section we consider how feedbacks within the mevalonate pathway
626 contribute to the robust control of cholesterol concentrations. Whilst in pre-
627 vious sections we have focused on the role of the global cholesterol-SREBP-
628 2 negative feedback, here we consider the effect of geranyl-PP, farnesyl-PP,
629 lanosterol and cholesterol regulating the degradation of HMGCR, and chole-
630 sterol regulating the degradation of squalene synthase, respectively.

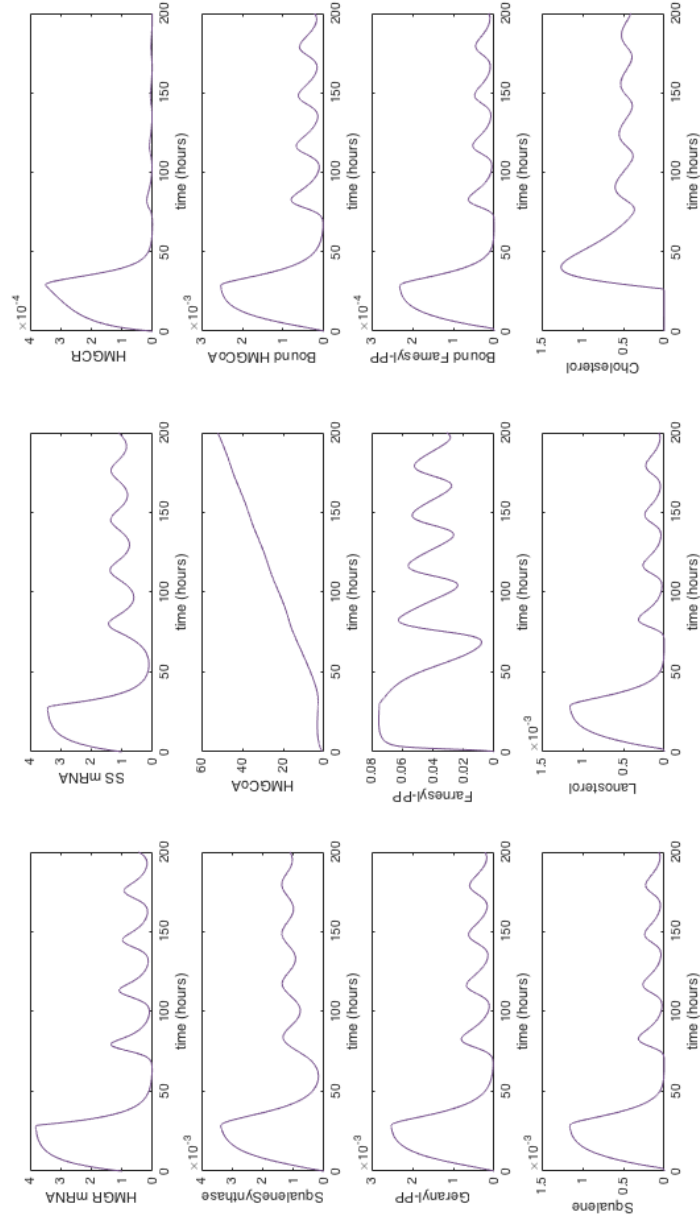


Figure 4: Solutions to the system of equations (34) to (46) for which periodic behaviour is exhibited. In this case $\kappa_1 = 1 \times 10^{-12}$, $\kappa_2 = 1 \times 10^{-12}$, $\kappa_3 = 3.74 \times 10^{-4}$, $\delta_8 = 0.1$, with all other parameters as in Table 2.

631 Given the complexity of the full pathway we began by considering the reduced
632 model shown in Figure 3. This allowed for initial examination of the effect of
633 the feedbacks on the core elements of the network (e.g. rate limiting steps and
634 core products), rather than each individual entity in the full pathway. We
635 identified each feedback in Figure 3 as: (1) $z \rightarrow u$ (cholesterol to HMGCR);
636 (2) $y \rightarrow u$ (farnesyl-PP to HMGCR); and (3) $z \rightarrow v$ (cholesterol to squalene
637 synthase).

638 We undertook numerical simulations of equations (55) - (60) using the MAT-
639 LAB solver ode15s, assuming $\epsilon = 0.1$ under the eight scenarios detailed in
640 Table 4; when all feedbacks were present, no feedbacks were present, each
641 feedback acted independently and pair-wise. We recorded the difference in
642 steady-state cholesterol concentration, measured as a percentage relative to
643 when all feedbacks were present, in Table 4.

644 The results in Table 4 clearly show that for fewer feedbacks steady-state
645 cholesterol concentrations increase. When no feedbacks are present, choles-
646 terol levels increase by 27.4% in comparison to when all feedbacks are present.
647 Individually, the feedback from farnesyl-PP onto HMGCR has the great-
648 est effect on regulating cholesterol levels, whereas those from cholesterol to
649 HMGCR and squalene synthase have the least similar effect. Interestingly
650 our results demonstrate that the feedbacks between cholesterol and HMGCR
651 and squalene synthase, respectively, together have just as tight a control on
652 cholesterol as that of the feedback from farnesyl-PP to HMGCR. The re-
653 sults of Table 4 also show that local positive feedbacks affecting the rates of
654 HMGCR and squalene synthase degradation act together with the two rate
655 limiting steps in which they are respectively involved, to tightly regulate the
656 concentration of cholesterol. Importantly, they are able to do so more di-
657 rectly and thus more rapidly, given less regulatory steps are involved, than
658 via the feedback between cholesterol and SREBP-2.

659 To test the robustness of the feedback responses, specifically the transient
660 concentration of cholesterol, we introduced a transient influx of cholesterol,
661 B in to z such that

$$B = \begin{cases} 1, & \text{for } 0.10 \leq t \leq 0.15, \\ 0 & \text{otherwise.} \end{cases} \quad (72)$$

662 under differing feedback scenarios.

Table 4: The percentage relative difference in steady-state cholesterol concentration for when different feedbacks are included compared to when all three feedbacks are in play for the reduced model of Figure 3. In the case of comparing feedbacks either individually or pairwise, the other feedbacks were turned off. Here: (1) $z \rightarrow u$ (cholesterol to HMGCR); (2) $y \rightarrow u$ (intermediate substrates to HMGCR); and (3) $z \rightarrow v$ (cholesterol to squalene synthase) as, defined in Figure 3.

Scenario	Corresponding weighting parameters	Percentage increase in steady-state cholesterol levels.
No feedbacks	$\delta_{uz} = 0 = \delta_{uy} = \delta_{vz}$.	27.4%
(1)	$\delta_{uz} = 1, \delta_{uy} = 0 = \delta_{vz}$.	12.6%
(2)	$\delta_{uz} = 0, \delta_{uy} = 1, \delta_{vz} = 0$.	1.6%
(3)	$\delta_{uz} = 0 = \delta_{uy}, \delta_{vz} = 1$.	12.9%
(1), (2)	$\delta_{uz} = 1 = \delta_{uy}, \delta_{vz} = 0$.	12.6%
(1), (3)	$\delta_{uz} = 1, \delta_{uy} = 0, \delta_{vz} = 1$.	1.6%
(2), (3)	$\delta_{uz} = 0, \delta_{uy} = 1 = \delta_{vz}$.	10.3%

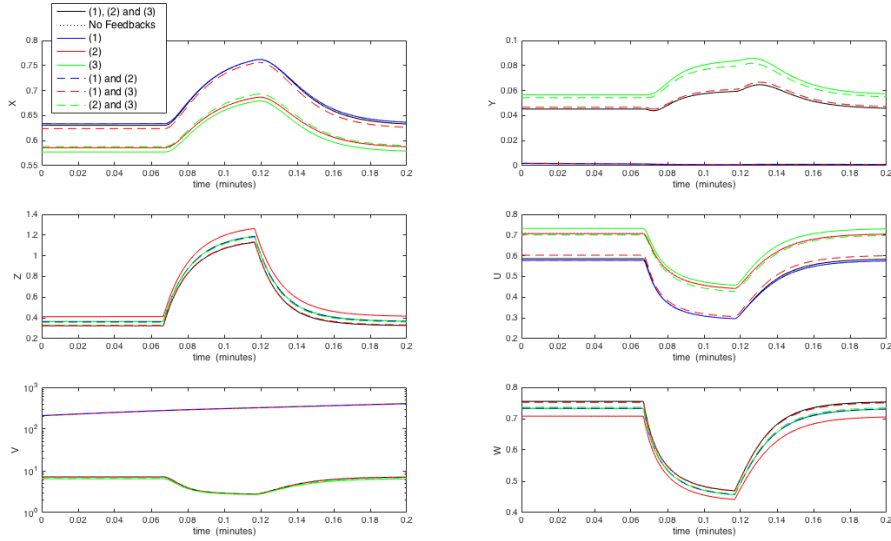


Figure 5: The impact of feedbacks on the reduced model of Figure 3 for the case where z (cholesterol) is increased for $0.10 < t < 0.15$. Equations (55)-(60) were solved for all parameter set equal to one with the exception of $\epsilon = 0.1$. Solutions were allowed to reach steady-state before the effect of turning each feedback off was investigated.

663 Figure 5 demonstrates that each of the feedbacks tightly regulate the concen-
664 trations of x , y and z and that varying combinations of them did not alter the
665 overall transient behaviour. Additionally in scenarios where feedback (3) was
666 turned off, levels of y (farnesyl-PP) were very low as more squalene synthase
667 is available to bind with farnesyl-PP to form squalene. This coupled with
668 the analysis undertaken in Section 6 showing if the concentration of squalene
669 synthase grows unbounded the rate limiting step between it and farnesyl-PP
670 acts to control the downstream concentrations of lanosterol and subsequently
671 cholesterol, demonstrates these two processes act together locally to tightly
672 regulate cholesterol levels in this section of the pathway.

673 We undertook the same analysis of each feedback on the full model of the
674 pathway, equations (34) to (46). We inhibited the feedbacks from: (1) choles-
675 terol to HMGCR degradation; (2) farnesyl-PP to HMGCR degradation; and
676 (3) cholesterol to squalene synthase degradation. We again conducted the
677 same eight scenarios detailed in Table 4 and found all scenarios show the same
678 transient behaviour in good agreement with the reduced model. The only
679 notable change was were switching feedback (2) off led to slightly higher lev-
680 els of HMGCR. This difference was not seen when feedback (3) was switched
681 on concurrently to feedback (2).

682 10. CYP51 inhibition

683 So far we have demonstrated that cholesterol biosynthesis via the mevalonate
684 pathway is a tightly regulated process; a result of two enzymatic rate limiting
685 steps coupled with local and global feedbacks within the signalling network.
686 In this section we show how these elements integrate together to ensure a
687 robust network response to the effect of the fungicide agent CYP51. CYP51
688 is known to inhibit post lanosterol production processes and is used in crop
689 protection as an anti-fungal agent. It acts by reducing cholesterol concen-
690 trations within the cell, thereby compromising cell wall integrity, ultimately
691 leading to cell death. Concerns exist that this inhibition is likely to lead to
692 increases in farnesyl-PP levels, thereby inducing unwanted side-effects within
693 other cell signalling cascades who share cross-talk with farnesyl-PP.

694 To investigate the effect of CYP51 inhibition on the pathway we first ran the
695 system of equations (34) to (46) to steady-state. Taking this as our starting

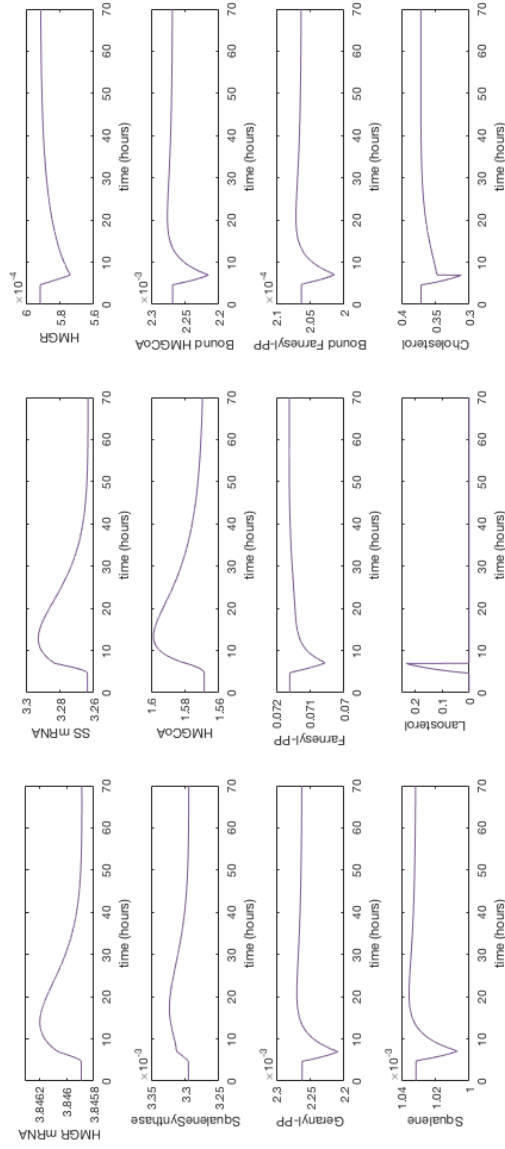


Figure 6: The effect of CYP51 inhibition on equations (34) to (46). Here $\mu_9 = 0$ at $\bar{t} = 5$ hours for 2 hours with $\kappa_3=0.075$, to simulate CYP51 inhibition as described by equation (73). Cholesterol concentrations decline which leads to a decrease in HMGCR levels as a result of the feedback between cholesterol and SREBP-2. Hence concentrations of geranyl-PP, farnesyl-PP and squalene all decline. All concentrations return to steady-state after CYP51 inhibition stops.

696 point we then simulated the effect of CYP51 inhibitors by letting

$$\mu_9 = \begin{cases} 0, & \text{for } 5 \leq t \leq 7, \\ 3.61 \times 10^2 & \text{otherwise.} \end{cases} \quad (73)$$

697 Results are shown in Figure 6. We see that CYP51 inhibition leads to a
698 sharp increase in lanosterol and decline in cholesterol concentrations. Here
699 we would expect an increase in HMGCR concentrations due to the rise in
700 HMGCR mRNA, however the sharp increase in lanosterol concentration
701 causes the degradation of HMGCR to be up-regulated, and so its concen-
702 tration subsequently declines. The reduction in HMGCR thus leads to a
703 decline in the central cascade products of geranyl-PP, farnesyl-PP and squa-
704 lene. As a result we see that the change in these central cascade products is
705 limited and that farnesyl-PP levels actually reduce when production of chole-
706 sterol from lanosterol is inhibited. We note that an increase in inhibition of
707 SREBP-2 by cholesterol ($\kappa_3 = 0.075$) was required in order to observe a
708 response in HMGCR mRNA and squalene synthase mRNA.

709 11. Summary and conclusions

710 We have formulated, parameterised and analysed a nonlinear ODE model
711 of the mevalonate cholesterol biosynthesis pathway. Our results show that
712 the pathway tightly regulates steady-state and transient cholesterol levels via
713 two rate limiting steps, internal local positive feedbacks affecting the rate of
714 degradation of certain products within the pathway and a global negative
715 feedback between cholesterol and SREBP-2.

716 A local sensitivity analysis of the model revealed a number of important reg-
717 ulatory points within the pathway. It highlighted that decreases in HMGCR
718 levels has the greatest impact on downstream cholesterol levels either via
719 variation in transcription or translation rates or the rate of HMGCR mRNA
720 or HMGCR degradation. Increasing products prior to farnesyl-PP interact-
721 ing with squalene synthase has a more significant effect on cholesterol levels
722 in contrast to those after the reaction, the rates at which geranyl-PP and
723 squalene are formed have the most significant effect. Altering the rate of
724 cholesterol esterification has a significant impact on HMGCR and squalene
725 synthase levels via the cholesterol SREBP-2 negative feedback loop.

726 Our sensitivity analysis also revealed the importance of the rate limiting en-
727 zyme substrate reactions of HMGCoA with HMGCR and farnesyl-PP with
728 squalene synthase, the latter augmented by separate analytical analysis of the
729 farnesyl-PP squalene synthase rate limiting step. The HMGCR-HMGCoA
730 reaction was found to be an important upstream regulator of all main path-
731 way products. That of farnesyl-PP and squalene synthase was found to
732 be important in not only regulating downstream production of squalene,
733 lanosterol and thus cholesterol, but in ensuring their levels did not increase
734 significantly if levels of farnesyl-PP and squalene synthase did.

735 Analysis of a reduced model of the full pathway, which captured the main
736 products and interactions between them, demonstrated that the system ex-
737 hibits one real stable steady-state. The global feedback between cholesterol
738 and SREBP-2 leads to monotonic, oscillatory and damped oscillatory be-
739 haviour, which agrees with the simplified HMGCR cholesterol regulatory
740 model of [2]. This result shows that the feedback between cholesterol and
741 SREBP-2 acts to globally regulate the dynamic pathway behaviour. This
742 is in contrast to internal positive feedbacks between geranyl-PP, farnesylPP,
743 lanosterol and the degradation of HMGCR and squalene synthase which our
744 analysis demonstrated act directly within the pathway to tightly regulate
745 overall cholesterol concentrations.

746 It is clear that feedbacks in the pathway act to control the dynamical re-
747 sponse, enzyme concentrations and hence the concentration of cholesterol.
748 The cholesterol-SREBP-2 feedback allows for cholesterol regulation of its own
749 production over a longer timescale than those from geranyl-PP, farnesyl-PP,
750 lanosterol and cholesterol to HMGCR and cholesterol to squalene synthase;
751 which respond directly within the pathway to any variation in cholesterol lev-
752 els. These direct responses alleviate the effect of further reactions in delaying
753 the reduction of the entity they are targeting in the pathway.

754 Further evidence of the system's robust network control via the integration
755 of two rate limiting steps and feedbacks was shown in the case of CYP51
756 inhibition. Simulations of CYP51 inhibition show the network response pre-
757 vents cytotoxic build up of central cascade products geranyl-PP, squalene and
758 farnesyl-PP. This is important since increased farnesyl-PP levels are linked
759 with several other signalling pathways and excessive amounts are thought
760 to cause tumours. In this way we have shown that CYP51 inhibitors would
761 have little effect on farnesyl-PP concentrations in the mevalonate pathway.

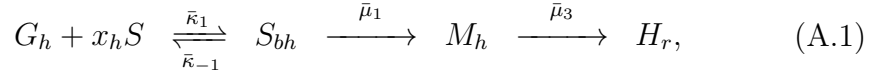
762 Given the importance of cholesterol synthesis in maintaining the integrity of
763 cell function for many cellular phenotypes, the results of the work here are in
764 many ways unsurprising. Cholesterol levels need to be tightly regulated, both
765 in response to internal cellular variations and external factors, e.g. disease or
766 dietary factors. Our work here has clearly demonstrated that the pathway is
767 robustly designed and includes a number of ‘fail safe’ type mechanisms in the
768 form of regulatory feedbacks and rate limiting steps which act in concert to
769 provide a robust regulatory system. These results are in agreement with the
770 work of August et al. [1] and Morgan et al. [25], who both demonstrated that
771 the cholesterol biosynthesis aspects of their models were robust to parameter
772 variation. The design of the network ensures that the integrity of cholesterol
773 levels is not greatly compromised, should one or more of these mechanisms
774 fail, thus ensuring cell survival is maintained.

775 **Acknowledgement**

776 FP acknowledges the support of a Engineering Physical Sciences Research
777 Council (EPSRC) UK CASE studentship in collaboration with Syngenta
778 (EP/P505682/1 & EP/J500501/1). MJT is grateful for the support of a
779 Research Council UK Fellowship (EP/C508777/1) during parts of the period
780 in which this work was undertaken.

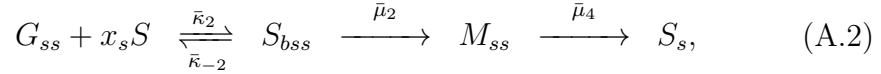
781 **Appendix A. Biochemical reaction details**

782 In order to formulate a mathematical model of the interactions shown in
 783 Figure 1 we first consider the biochemical details of each reaction. The
 784 binding of SREBP-2 to HMGCR DNA and subsequent mRNA and protein
 785 formation is governed by



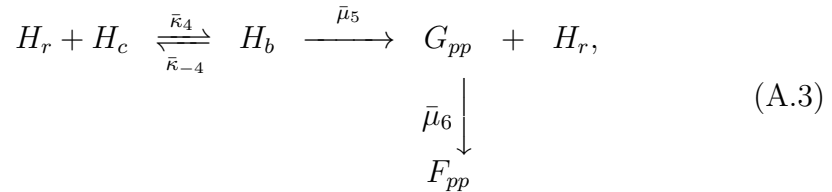
786 where HMGCR free DNA is represented by G_h , S is SREBP-2, S_{bh} is SREBP-
 787 2 bound to the DNA, M_h is HMGCR mRNA and H_r is HMGCR. The
 788 constant reaction rates $\bar{\kappa}_1$ and $\bar{\kappa}_{-1}$ represent the binding and unbinding of
 789 SREBP-2 and DNA protein respectively, $\bar{\mu}_1$ is the rate of transcription of
 790 HMGCR mRNA and $\bar{\mu}_3$ is the rate of HMGCR translation. Finally x_h is the
 791 number of binding sites on the DNA that SREBP-2 must bind to.

792 Binding of SREBP-2 to squalene synthase DNA and subsequent mRNA and
 793 protein formation is governed by



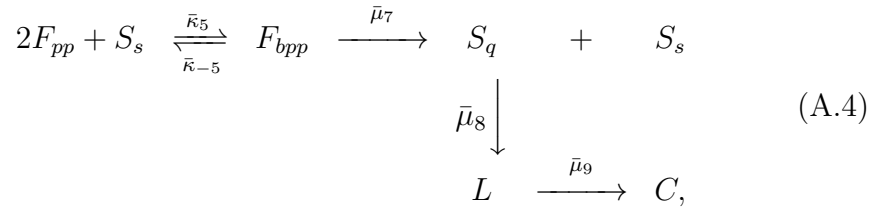
794 where free DNA binding sites responsible for squalene synthase synthesis is
 795 represented by G_{ss} , S_{bss} is SREBP-2 bound to the DNA, M_{ss} is squalene
 796 synthase mRNA and S_s is squalene synthase. The constant reaction rates
 797 $\bar{\kappa}_2$ and $\bar{\kappa}_{-2}$ represent the binding and unbinding of SREBP-2 and DNA re-
 798 spectively, $\bar{\mu}_2$ is the rate of transcription of mRNA responsible for squalene
 799 synthase and $\bar{\mu}_4$ is the rate of translation of squalene synthase from mRNA.
 800 Finally x_s is the number of binding sites on the DNA that SREBP-2 must
 801 bind to.

802 Binding of HMGCR and HMGCoA and subsequent production of geranyl-PP
 803 and farnesyl-PP is governed by



804 where free HMGCoA is represented by H_c , H_b is HMGCR bound to HMG-
805 CoA, G_{pp} is geranyl-PP and F_{pp} is farnesyl-PP. The constant reaction rates
806 $\bar{\kappa}_4$ and $\bar{\kappa}_{-4}$ represent binding and unbinding of HMGCR and HMGCoA re-
807 spectively, $\bar{\mu}_5$ is the rate of production of geranyl-PP and $\bar{\mu}_6$ is the rate of
808 production of farnesyl-PP.

809 Two molecules of farnesyl-PP bind to one molecule of squalene synthase for
810 the subsequent production of squalene, lanosterol and cholesterol such that



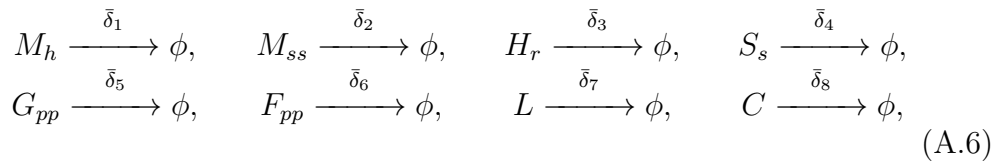
811 where bound farnesyl-PP and squalene synthase is represented by $F_{b_{pp}}$, S_q is
812 squalene, L is lanosterol and C is cholesterol. The constant reaction rates $\bar{\kappa}_5$
813 and $\bar{\kappa}_{-5}$ denote binding and unbinding of squalene synthase and farnesyl-PP
814 respectively, $\bar{\mu}_7$ is the rate of squalene production, $\bar{\mu}_8$ is the rate of lanosterol
815 production $\bar{\mu}_9$ that of cholesterol.

816 The negative regulation of SREBP-2 by cholesterol is governed by



817 where bound cholesterol and SREBP-2 is represented by C_b , the constant
818 reaction rates $\bar{\kappa}_3$ and $\bar{\kappa}_{-3}$ represent the binding and unbinding of cholesterol
819 and SREBP-2, respectively. Finally x_c is the number of binding sites that
820 must be occupied by cholesterol on SREBP-2 to inactivate SREBP-2.

821 Each degradation process is described by



822 where δ_i ($i \in [1, \dots, 8]$) are the rates of degradation of each mRNA, protein
823 and enzyme, respectively.

824 **Appendix B. Model reduction**

825 We begin by observing three conservation relations. Firstly, the total amount
826 of DNA within a cell remains constant such that

$$\bar{g}_h + \bar{s}_{bh} = \bar{g}_{h0} \quad \text{and} \quad \bar{g}_{ss} + \bar{s}_{bss} = \bar{g}_{ss0}, \quad (\text{B.1})$$

827 which are formed from the addition and integration (with respect to time)
828 of equations (1) and (4), and (2) and (5), respectively.

829 The total amount of SREBP-2 in a cell is also constant which similarly gives

$$\bar{s} + \bar{c}_b = \bar{s}_0, \quad (\text{B.2})$$

830 using equations (3) and (18).

We assume the following reactions occur on a faster timescale than others in the signalling cascade and as such invoke the quasi-steady-state approximation. We assume DNA-transcription factor binding is rapid [20, 2] such that from equation (4)

$$\bar{\kappa}_1 \bar{s}^{x_h} (\bar{g}_{h0} - \bar{s}_{bh}) - \bar{\kappa}_{-1} \bar{s}_{bh} \approx 0,$$

831 where we have substituted for \bar{g}_h using the first conservation relationship in
832 equation (B.1). This result can be re-arranged for \bar{s}_{bh} to give

$$\bar{s}_{bh} \approx \frac{\bar{g}_{h0} \bar{s}^{x_h}}{\bar{s}^{x_h} + \bar{K}_1}, \quad (\text{B.3})$$

833 with $\bar{K}_1 = \left(\frac{\bar{\kappa}_{-1}}{\bar{\kappa}_1} \right)^{\frac{1}{x_h}}$.

834 Using the second conservation relationship in equation (B.1) and applying
835 the same assumption to equation (5) yields

$$\bar{s}_{bss} \approx \frac{\bar{g}_{ss0} \bar{s}^{x_s}}{\bar{s}^{x_s} + \bar{K}_2}, \quad (\text{B.4})$$

836 with $\bar{K}_2 = \left(\frac{\bar{\kappa}_{-2}}{\bar{\kappa}_2} \right)^{\frac{1}{x_s}}$.

837 Finally we assume that cholesterol-SREBP-2 binding is also rapid such that
838 from equation (3)

$$\bar{s} \approx \frac{\bar{K}_3^{x_c} \bar{s}_0}{\bar{c}^{x_c} + \bar{K}_3^{x_c}} = \frac{\bar{s}_0}{1 + \left(\frac{\bar{c}}{\bar{K}_3} \right)^{x_c}}, \quad (\text{B.5})$$

839 with $\bar{K}_3 = \left(\frac{\bar{k}-3}{\bar{K}_3}\right)^{\frac{1}{x_c}}$. This relationship can subsequently be used to express
 840 \bar{s}_{bh} and \bar{s}_{bss} in terms of c .

841 Using the results of equations (B.3), (B.4) and (B.5) we can simplify equa-
 842 tions (6) and (7) to

$$\frac{d\bar{m}_h}{d\bar{t}} = \frac{\bar{\mu}_1^*}{1 + \left(\frac{\bar{K}_1(1+(\frac{\bar{c}}{\bar{K}_3})^{x_c})}{\bar{s}_0}\right)^{x_h}} - \bar{\delta}_1\bar{m}_h, \quad (\text{B.6})$$

843 and

$$\frac{d\bar{m}_{ss}}{d\bar{t}} = \frac{\bar{\mu}_2^*}{1 + \left(\frac{\bar{K}_2(1+(\frac{\bar{c}}{\bar{K}_3})^{x_c})}{\bar{s}_0}\right)^{x_s}} - \bar{\delta}_2\bar{m}_{ss}, \quad (\text{B.7})$$

844 where $\bar{\mu}_1^* = \bar{\mu}_1\bar{g}_{h0}$ and $\bar{\mu}_2^* = \bar{\mu}_2\bar{g}_{ss0}$.

Equation (31) is derived from equations (3), (4), (5) and (17), respectively,
 such that

$$\frac{d}{d\bar{t}}(\bar{s} + x_h\bar{s}_{bh} + x_s\bar{s}_{bss} - \bar{c}/x_c) = \frac{\bar{\mu}_9\bar{l} - \bar{\delta}_8\bar{c}}{x_c}$$

which leads to

$$(1 - x_c(\bar{s}' + x_h\bar{s}'_{bh} + x_s\bar{s}'_{bss}))\frac{d\bar{c}}{d\bar{t}} = \bar{\mu}_9\bar{l} - \bar{\delta}_8\bar{c},$$

845 via the chain rule, where ' denotes differentiation with respect to \bar{c} such that
 846 from (B.5), (B.3) and (B.4) we have

$$\frac{d\bar{s}}{d\bar{c}} = \frac{-\bar{s}_0x_c\left(\frac{\bar{c}}{\bar{K}_3}\right)^{x_c}}{\bar{c}\left(1 + \left(\frac{\bar{c}}{\bar{K}_3}\right)^{x_c}\right)^2}, \quad (\text{B.8})$$

847

$$\frac{d\bar{s}_{bh}}{d\bar{c}} = \frac{d\bar{s}_{bh}}{d\bar{s}}\frac{d\bar{s}}{d\bar{c}} = \frac{x_h\bar{g}_{h0}\bar{K}_1^{x_h}\bar{s}^{x_h-1}}{(\bar{s}^{x_h} + \bar{K}_1^{x_h})^2}\frac{d\bar{s}}{d\bar{c}} \quad (\text{B.9})$$

848 and

$$\frac{d\bar{s}_{bss}}{d\bar{c}} = \frac{d\bar{s}_{bss}}{d\bar{s}}\frac{d\bar{s}}{d\bar{c}} = \frac{x_s\bar{g}_{ss0}\bar{K}_2^{x_s}\bar{s}^{x_s-1}}{(\bar{s}^{x_s} + \bar{K}_2^{x_s})^2}\frac{d\bar{s}}{d\bar{c}}, \quad (\text{B.10})$$

849 respectively. Here \bar{g}_{h0} and \bar{g}_{ss0} are the total concentration of HMGCR and
 850 squalene synthase DNA, respectively, in a cell.

851 **Appendix C. Parameter details**

852 In this section we detail, where relevant, calculations used to estimate the
853 parameters detailed in Table 1.

854 **\bar{m}_{h0} - Initial concentration of HMGCR mRNA:** Ruddling et al. [30]
855 details copy numbers of mRNA found in human liver cells under basal con-
856 ditions. So we take a value of 30 copies of HMGCR mRNA per cell i.e. per
857 10^{-9} ml. So

$$\frac{30 \text{ molecules}}{1 \times 10^{-9} \text{ ml}} = 3.0 \times 10^{10} \text{ molecules/ml.}$$

858 This value was then refined using local sensitivity analysis to give $\bar{m}_{h0} =$
859 3.0×10^9 molecules/ml.

860 **\bar{m}_{ss0} - Initial concentration of squalene synthase mRNA:** Ruddling
861 et al. [30] details copy numbers of mRNA found in human liver cells under
862 basal conditions. So we take a value of 30 copies of squalene synthase mRNA
863 per cell i.e. per 10^{-9} ml. So

$$\frac{30 \text{ molecules}}{1 \times 10^{-9} \text{ ml}} = 3.0 \times 10^{10} \text{ molecules/ml.}$$

864 This value was then refined using local sensitivity analysis to give $\bar{m}_{ss0} =$
865 3.0×10^9 molecules/ml.

866 **\bar{s}_{sT} - Total concentration of squalene synthase:** One liver cell contains
867 300pg/cell protein and has a volume of 10^{-9} ml. Bruenger and Rilling [5]
868 state there are 4.2 nmol of squalene synthase per gram of wet tissue such
869 that

$$4.2 \times 10^{-9} \text{ mol/g tissue} \times 6.022 \times 10^{23} \text{ molecules/mol}$$

870 which gives

$$\frac{2.53 \times 10^{15} \text{ molecules/g} \times 1.00 \times 10^{-12}}{10^{-9} \text{ ml}} = 7.59 \times 10^{14} \text{ molecules/ml.}$$

871 **\bar{h}_{cT} - Total concentration of HMGCoA:** One liver cell contains approxi-
872 mately 300pg/cell protein and has volume 10^{-9} ml/cell. The molecular weight
873 of HMGCoA is 199.659 g/mol according to human metabolic database [38].
874 Then we know

$$\frac{300 \times 10^{-12} \text{ g}}{199.659 \text{ g/mol}} = 3.29 \times 10^{-13} \text{ mol/cell.}$$

875 So we have, per cell, $3.29 \times 10^{-13} \text{mol}/10^{-9} \text{ml} = 3.92 \times 10^{-4} \text{mol/ml}$. Applying
 876 Avagadro's number we can find the number of molecules per ml

$$3.92 \times 10^{-4} \text{mol/ml} \times 6.022 \times 10^{23} \text{ molecules/mol} = 1.98 \times 10^{20} \text{ molecules/ml.}$$

877 Segel (1993) [33] states a cell contains an average of 1000 enzymes, so we have
 878 $9.04 \times 10^{14} \text{ molecules/ml}$. This value was then refined using local sensitivity
 879 analysis to give $\bar{h}_{cT} = 1.98 \times 10^{15} \text{ molecules/ml}$.

880 **$\bar{g}_{h0}, \bar{g}_{ss0}$ - HMGCR and squalene synthase gene concentration:** The
 881 molecular weight of the HMGCR gene is 97,476 Da [41], whilst that of the
 882 human genome is $2 \times 10^{12} \text{Da}$ [42]. The total quantity of DNA in a cell
 883 weighs 7pg, such that that of HMGCR is $3.41 \times 10^{-7} \text{pg}$. Observing that 1 Da
 884 is equivalent to 1g/mol and assuming the volume of a cell is 1 nml, we have

$$\frac{3.41 \times 10^{-7} \text{ pg} \times 6.023 \times 10^{23} \text{ molecules/mol}}{97,476 \text{ g/mol} \times 1 \text{ nml}} = 2.11 \times 10^9 \text{ molec/ml.}$$

885 We likewise assume the squalene synthase gene (with no further details avail-
 886 able) is the same concentration.

887 **$\bar{\mu}_1^*$ - Rate of HMGCR mRNA transcription:** Darzacq et al. [8] states
 888 12 bases are transcribed per second. Goldstein and Brown [12] say one
 889 HMGC_oA-R gene is 24826 bases long. Therefore we have

$$\frac{24826 \text{ bases}}{12 \text{ bases/s}} = 2068.83\text{s.}$$

890 We add 30 minutes to account for post transcriptional processing steps of
 891 mRNA cleavage giving 3868.83s. So for one gene we have

$$\frac{1 \text{ molecule}}{3868.83\text{s}} = 2.58 \times 10^{-4} \text{ molecules/s.}$$

892 A liver cell is somatic and hence diploid meaning it contains contains two
 893 genes, so we have

$$2.58 \times 10^{-4} \text{ molecules/s} \times 2 = 5.17 \times 10^{-4} \text{ molecules/s.}$$

894 The average cell volume is 1pl = $1 \times 10^{-9} \text{ml}$ so the rate of transcription is
 895 given by

$$\frac{5.17 \times 10^{-4} \text{ molecules/s}}{1 \times 10^{-9} \text{ml}}$$

896 giving $\bar{\mu}_1^* = 5.17 \times 10^5$ molecules/ml/s.

897 **$\bar{\mu}_2^*$ - Rate of squalene synthase mRNA transcription:** Darzacq et al. [8]
898 states 12 base pairs are transcribed per second. Tansey & Shechter [37] say
899 one human squalene synthase gene is over 30000 bases long. Therefore we
900 have

$$\frac{30000 \text{ bases}}{12 \text{ bases/s}} = 2500\text{s}.$$

901 We add 30 minutes to account for post transcriptional processing steps of
902 mRNA cleavage giving 4300 thus for one gene we have

$$\frac{1 \text{ molecule}}{4300\text{s}} = 2.33 \times 10^{-4} \text{ molecules/s}.$$

903 A liver cell is somatic and hence diploid meaning it contains contains two
904 genes, so we have

$$2.33 \times 10^{-4} \text{ molecules/s} \times 2 = 4.65 \times 10^{-4} \text{ molecules/s}.$$

905 The average cell volume is 1pl = 1×10^{-9} ml so the rate of transcription is
906 given by

$$\frac{4.65 \times 10^{-4} \text{ molecules/s}}{1 \times 10^{-9}\text{ml}}$$

907 giving $\bar{\mu}_2^* = 4.65 \times 10^5$ molecules/ml/s.

908 **$\bar{\mu}_3$ - Rate of HMGCR translation:** Trachsel [39] states 6 amino acids are
909 translated per second. One amino acid is encoded by 3 bases or nucleotides.
910 HMGCR mRNA transcript has 4475 bases (Goldstein & Brown [12]). Hence
911 transcription takes:

$$\frac{4475 \text{ bases}}{6 \text{ amino acids/s} \times 3 \text{ amino acids/base}} = 248.61\text{s},$$

912 We add 60 minutes to account for the initiation of this process

$$3848.61\text{s}.$$

913 Then per ribosome we have

$$\frac{1 \text{ molecule}}{3848.61\text{s}} = 2.60 \times 10^{-4} \text{ molecules/s/ribosome}.$$

914 A ribosome can only attach every 35 bases do to its size meaning 1 mRNA
 915 molecule has 127.86 ribosomes attached.
 916 Then per mRNA molecule we have:

$$2.60 \times 10^{-4} \text{ molecules/s/ribosome} \times 127.86 \text{ ribosomes/molecule}$$

917 giving $\bar{\mu}_3 = 3.32 \times 10^{-2} \text{ /s}$.

918 **$\bar{\mu}_4$ - Rate of squalene synthase translation:** Trachsel [39] states 6 amino
 919 acids are translated per second. One amino acid is encoded by 3 bases
 920 or nucleotides. Jiang et al. [36] state that one squalene synthase mRNA
 921 transcript contains 2502 bases. Hence transcription takes:

$$\frac{2502 \text{ bases}}{6 \text{ amino acids/s} \times 3 \text{ amino acids/base}} = 139\text{s,}$$

922 We add 60 minutes to account for the initiation of this process

$$3739\text{s.}$$

923 Then per ribosome we have

$$\frac{1 \text{ molecule}}{3739\text{s}} = 2.67 \times 10^{-4} \text{ molecules/s/ribosome.}$$

924 A ribosome can only attach every 35 bases do to its size meaning 1 mRNA
 925 molecule has 71.49 ribosomes attached.
 926 Then per mRNA molecule we have:

$$2.67 \times 10^{-4} \text{ molecules/s/ribosome} \times 71.49 \text{ ribosome/molecule}$$

927 giving $\bar{\mu}_4 = 1.91 \times 10^{-2} \text{ /s}$.

928 **$\bar{\mu}_5$ - Rate of geranyl-PP synthesis:** Tanaka et al. [47] tell us that liver
 929 microsomes form 52 pmol mevalonate per minute per mg protein. Istvan et
 930 al. [15] say HMGCR is tetrameric arranged in 2 dimer, with 4 active sites,
 931 has molecular weight 199812 Da. The activity of the enzyme is where

$$52 \times 10^{-12} \text{ mol/min/mg protein} \approx 52 \times 10^{-12} \times N_A.$$

932 $N_A = 6.022 \times 10^{23}$ is Avagadro's constant. So we have

$$52 \times 10^{-12} \text{ mol/min/mg protein} \times 6.022 \times 10^{23} \text{ molecules/mol}$$

933

$$= 3.13 \times 10^{13} \text{ molecules/min/mg protein.}$$

934 Segel [33] says there's 1000 different enzymes in a cell, so for 1 mg of protein
935 we have

$$\frac{1 \times 10^{-3} \text{g}}{199812 \text{g/mol} \times 1000} = 5.00 \times 10^{-12} \text{mol.}$$

936 Given there are 4 active sites per HMGA-CoA Reductase enzyme, there are
937 2.00×10^{-11} moles of enzyme active sites in 1 mg of protein. Given the specific
938 activity of an enzyme we find $\bar{\mu}_5$ is equal to

$$\frac{52 \times 10^{-12} \text{ mol/min/mg}}{2.00 \times 10^{11} \text{mol/mg}} = 2.60 \text{min}$$

939 giving $\bar{\mu}_5 = 4.33 \times 10^{-2} / \text{s}$.

940 **$\bar{\mu}_6, \bar{\mu}_8$ and $\bar{\mu}_9$ - Rates of farnesyl-PP, lanosterol and cholesterol syn-**
941 **thesis:** Since the value for $\bar{\mu}_5$ is used to describe cholesterol production from
942 HMGCR, we can assume all steps in between must occur at the same rate
943 or faster. Therefore we set $\bar{\mu}_6, \bar{\mu}_8$ and $\bar{\mu}_9$ equal to $4.33 \times 10^{-2} / \text{s}$.

944 **$\bar{\mu}_7$ - Rate of squalene synthesis.** Since the value for $\bar{\mu}_5$ is used to describe
945 cholesterol production from HMGCR, we can assume all steps in between
946 must occur at the same rate or faster. Therefore as an estimate we set $\bar{\mu}_7$
947 equal to $4.33 \times 10^{-2} / \text{s}$. This value was then refined using local sensitivity
948 analysis to give $\bar{\mu}_7 = 2.17 \times 10^{-1} / \text{s}$.

949 **\bar{K}_1 - Disassociation constant of SREBP-2 for HMGCR DNA:** Yang
950 and Swartz [29] quantified DNA binding affinities to other transcription fac-
951 tors at 54.2 nmol. We convert this value into units of molecules/ml by the
952 use of Avogadro's constant.

$$\frac{100 \times 10^{-9} \text{ moles}}{1000 \text{ml}} \times 6.022 \times 10^{23} \text{ molecules/mol} = 3.26 \times 10^{13} \text{ molecules/ml.}$$

953 This value was then refined using local sensitivity analysis to give $\bar{K}_1 =$
954 8.21×10^{12} molecules/ml.

955 **\bar{K}_2 - Disassociation constant of SREBP-2 for squalene synthase**
956 **DNA:** This was assumed equivalent to that of SREBP-2 for HMGCR DNA,
957 i.e. 3.26×10^{13} molecules/ml. The value was then refined using local sensi-
958 tivity analysis to give $\bar{K}_2 = 8.21 \times 10^{12}$ molecules/ml.

959 **\bar{K}_3 - Disassociation constant of SREBP-2 for cholesterol:** Radhakrishnan et al. [46] state the binding reaction between cholesterol and SCAP
 960 is saturable and half-maximal binding occurs at approximately 100 nmol.
 961 We convert this value into units of molecules/ml by the use of Avogadro's
 962 constant.
 963

$$\frac{100 \times 10^{-9} \text{ moles}}{1000 \text{ ml}} \times 6.022 \times 10^{23} \text{ molecules/mol} = 6.02 \times 10^{13} \text{ molecules/ml,}$$

964 as an estimate we took $\bar{K}_3 = O(10^{14})$. This value was then refined using
 965 local sensitivity analysis to give $\bar{K}_3 = 1.49 \times 10^{16}$ molecules/ml.

966 **$\bar{\kappa}_4$ and $\bar{\kappa}_{-4}$ - Forward and reverse rates of HMGCR binding to HMG-**
 967 **CoA:** These values were initially informed by assuming the ratio of $\bar{\kappa}_4/\bar{\kappa}_{-4}$
 968 were the same order as those of \bar{K}_1 , \bar{K}_2 and \bar{K}_3 . We then assumed $\bar{\kappa}_{-4} \ll \bar{\kappa}_4$
 969 whereby we took an initial estimate of $\bar{\kappa}_{-4} = 1 \times 10^{-3}/\text{s}$. These values were
 970 then adjusted, via a sensitivity analysis, to give the required steady-state
 971 cholesterol levels. This resulted in values of $\bar{\kappa}_4 = 1.39 \times 10^{-16}$ ml/molecules
 972 s and $\bar{\kappa}_{-4} = 1.75 \times 10^{-7}$ /s.

973 **$\bar{\kappa}_5/\bar{\kappa}_5$ - Forward and reverse rates of farnesyl-PP binding to squalene**
 974 **synthase:** These values were obtained in a similar manner to those of $\bar{\kappa}_4$
 975 and $\bar{\kappa}_{-4}$. This led to $\bar{\kappa}_5 = 1.76 \times 10^{-30}$ ml/molecule s and $\bar{\kappa}_{-5} = 1.75 \times 10^{-5}$
 976 /s.

977 **\bar{K}_6 , \bar{K}_7 , \bar{K}_8 , \bar{K}_9 and \bar{K}_{10} - Michaelis-Menten constants of geranyl-PP,**
 978 **farnesyl-PP, lanosterol and cholesterol for HMGCR degradation**
 979 **and cholesterol for squalene synthase degradation, respectively:**
 980 These were determined as the half-maximal values which produced a sig-
 981 moidal type response for each of the respective cascade products.

982 **$\bar{\delta}_1$ - Degradation rate of HMGCR mRNA.** Degradation rates of proteins
 983 and mRNAs are based on their half lives, derived from an exponential decay
 984 model. Wilson and Deeley [3] state HMGCR mRNA has a half life of 4.3
 985 hours, measured in Hep G2 cells, giving $\bar{\delta}_1 = \ln 2/15480\text{s} = 4.48 \times 10^{-5}/\text{s}$.

986 **$\bar{\delta}_2$ - Degradation rate of squalene synthase mRNA:** This was assumed
 987 equivalent to that of HMGCR mRNA.

988 **$\bar{\delta}_3$ - Degradation of HMGCR:** Brown et al. [44] found HMGCR protein
 989 has a half life of 3 hours, measured in human fibroblast cells, such that
 990 $\bar{\delta}_3 = \ln 2/10800\text{s} = 6.42 \times 10^{-5}/\text{s}$.

991 $\bar{\delta}_4$ - **Squalene synthase degradation rate:** This was assumed equivalent
992 to that of HMGCR.

993 $\bar{\delta}_5$, $\bar{\delta}_6$ and $\bar{\delta}_7$ - **Degradation rates of geranyl-PP, farnesyl-PP and**
994 **lanosterol:** These were assumed equivalent to that of cholesterol.

995 $\bar{\delta}_8$ - **Cholesterol degradation rate:** We utilise the value previously derived
996 in Bhattacharya et al. [2] of 1.20×10^{-4} /s.

997 $\bar{\omega}$ - **HMGCoA production rate:** This value has been determined from our
998 sensitivity analysis to be 3.895×10^{11} molec./ml. The value has been found to
999 ensure enough cholesterol is produced.

1000 x_h - **Number of binding sites for SREBP-2 on HMGCR DNA:** Vallett
1001 et al. [28] state a value of 3.

1002 x_s - **Number of binding sites for SREBP-2 on squalene synthase**
1003 **DNA:** Without further evidence we assume this is 1.

1004 x_c - **Number of binding sites on SREBP-2 for cholesterol:** Radhakrishnan
1005 et al. [46, 16] state a value of 4.

1006 References

1007 [1] August, E., Parker, K., Barahona, M., 2007. A dynamical model of
1008 lipoprotein metabolism. *Bulletin of Mathematical Biology* 69 (4), 1233–
1009 1254.

1010 [2] Bhattacharya, B., Sweby, P., Minihane, A.-M., Jackson, K., Tindall,
1011 M., 2014. A mathematical model of the sterol regulatory element bind-
1012 ing protein 2 cholesterol biosynthesis pathway. *Journal of Theoretical*
1013 *Biology* 349, 150–162.

1014 [3] Brown, M., Dana, S., Goldstein, J., 1974. Regulation of 3-hydroxy-3-
1015 methylglutaryl coenzyme A reductase activity in cultured human fibrob-
1016 lasts comparison of cells from a normal subject and from a patient with
1017 homozygous familial hypercholesterolemia. *Journal of Biological Chem-*
1018 *istry* 249 (3), 789–796.

1019 [4] Brown, M., Goldstein, J., 1980. Multivalent feedback regulation of HMG
1020 CoA reductase, a control mechanism coordinating isoprenoid synthesis
1021 and cell growth. *Journal of Lipid Research* 21 (5), 505–517.

- 1022 [5] Bruenger, E., Rilling, H., 1988. Determination of isopentenyl diphos-
1023 phosphate and farnesyl diphosphate in tissue samples with a comment on sec-
1024 ondary regulation of polyisoprenoid biosynthesis. *Analytical Biochem-*
1025 *istry* 173 (2), 321–327.
- 1026 [6] Buhaescu, I., Izzedine, H., 2007. Mevalonate pathway: a review of clin-
1027 ical and therapeutical implications. *Clinical Biochemistry* 40 (9), 575–
1028 584.
- 1029 [7] Cole, S., Vassar, R., 2006. Isoprenoids and alzheimer’s disease: A com-
1030 plex relationship. *Neurobiology of Disease* 22, 209–222.
- 1031 [8] Darzacq, X., Shav-Tal, Y., de Turris, V., Brody, Y., Shenoy, S., Phair,
1032 R., Singer, R., 2007. In vivo dynamics of RNA polymerase II transcrip-
1033 tion. *Nature Structural & Molecular Biology* 14 (9), 796–806.
- 1034 [9] DeBose-Boyd, R., 2008. Feedback regulation of cholesterol synthesis:
1035 sterol-accelerated ubiquitination and degradation of hmg coa reductase.
1036 *Cell Research* 18, 609–21.
- 1037 [10] Foresti, O., Ruggiano, A., Hannibal-Bach, H., Ejsing, C., Carvalho,
1038 P., 2013. Sterol homeostasis requires regulated degradation of squalene
1039 monooxygenase by the ubiquitin ligase Doa10/Teb4. *Elife* 2, e00953.
- 1040 [11] Gaylor, J. L., 2002. Membrane-bound enzymes of cholesterol synthesis
1041 from lanosterol. *Biochemical and biophysical research communications*
1042 292 (5), 1139–1146.
- 1043 [12] Goldstein, J., Brown, M., 1984. Progress in understanding the LDL
1044 receptor and HMG-CoA reductase, two membrane proteins that regulate
1045 the plasma cholesterol. *Journal of Lipid Research* 25 (13), 1450–1461.
- 1046 [13] Goldstein, J., Brown, M., 1990. Regulation of the mevalonate pathway.
1047 *Nature* 343 (6257), 425–30.
- 1048 [14] Hampton, R., 2002. Proteolysis and sterol regulation. *Annual Review of*
1049 *Cell and Developmental Biology* 18, 345–78.
- 1050 [15] Istvan, E., Palnitkar, M., Buchanan, S., Deisenhofer, J., 2000. Crys-
1051 tal structure of the catalytic portion of human HMG-CoA reductase:
1052 insights into regulation of activity and catalysis. *The EMBO Journal*
1053 19 (5), 819–830.

- 1054 [16] Jackson, K., Maitin, V., Leake, D., Yaqoob, P., Williams, C., 2006.
1055 Saturated fat-induced changes in Sf 60–400 particle composition reduces
1056 uptake of LDL by HepG2 cells. *Journal of Lipid Research* 47 (2), 393–
1057 403.
- 1058 [17] Jiang, G., McKenzie, T., Conrad, D., Shechter, I., 1993. Transcriptional
1059 regulation by lovastatin and 25-hydroxycholesterol in HepG2 cells and
1060 molecular cloning and expression of the cDNA for the human hepatic
1061 squalene synthase. *Journal of Biological Chemistry* 268 (17), 12818–
1062 12824.
- 1063 [18] Kellner-Weibel, G., Geng, Y., Rothblat, G., 1999. Cytotoxic cholesterol
1064 is generated by the hydrolysis of cytoplasmic cholesteryl ester and trans-
1065 ported to the plasma membrane. *Atherosclerosis* 146, 309–19.
- 1066 [19] Kervizic, G., Corcos, L., 2008. Dynamical modeling of the choles-
1067 terol regulatory pathway with boolean networks. *BMC Systems Biology*
1068 2 (99), doi: 10.1186/1752-0509-2-99.
- 1069 [20] Lickwar, C. R., Mueller, F., Hanlon, S. E., McNally, J. G., Lieb, J. D.,
1070 2012. Genome-wide protein-DNA binding dynamics suggest a molecular
1071 clutch for transcription factor function. *Nature* 484 (7393), 251–255.
- 1072 [21] Matlab, Release 2016b. The MathWorks. Natick, Massachusetts, United
1073 States.
- 1074 [22] Mazein, A., Watterson, S., Hsieh, W., WJ, G., P, G., 2013. A compre-
1075 hensive machine-readable view of the mammalian cholesterol biosynthe-
1076 sis pathway. *Biochemical Pharmacology* 86 (1), 56–66.
- 1077 [23] Menegola, E., Broccia, M., Di Renzo, F., E, G., 2006. Postulated
1078 pathogenic pathway in triazole fungicide induced dysmorphogenic ef-
1079 fects. *Reproductive Toxicology* 260 (2), 186–95.
- 1080 [24] Michaelis, L., Menten, M., 1913. Die kinetik der invertinwirkung. *Bio-
1081 chemische Zeitschrift* 49 (333-369), 352.
- 1082 [25] Morgan, A., Mooney, K., Wilkinson, S., Pickles, N., MT., M. A., 2016.
1083 Mathematically modelling the dynamics of cholesterol metabolism and
1084 ageing. *Biosystems* 145, 19–32.

- 1085 [26] Murphy, L., Moore, T., S, N., 2012. Propiconazole-enhanced hepatic cell
1086 proliferation is associated with dysregulation of the cholesterol biosyn-
1087 thesis pathway leading to activation of Erk1/2 through Ras farnesylation.
1088 *Toxicology and Applied Pharmacology* 260 (2), 146–54.
- 1089 [27] Murray, J., 2002. *Mathematical Biology I: An Introduction*. Springer,
1090 New York, USA.
- 1091 [28] Radhakrishnan, A., Goldstein, J., McDonald, J., Brown, M., 2008.
1092 Switch-like control of SREBP-2 transport triggered by small changes
1093 in ER cholesterol: a delicate balance. *Cell Metabolism* 8 (6), 512–521.
- 1094 [29] Radhakrishnan, A., Sun, L.-P., Kwon, H., Brown, M., Goldstein, J.,
1095 2004. Direct binding of cholesterol to the purified membrane region of
1096 SCAP: mechanism for a sterol-sensing domain. *Molecular Cell* 15 (2),
1097 259–268.
- 1098 [30] Rudling, M., Angelin, B., Ståhle, L., Reihner, E., Sahlin, S., Olivecrona,
1099 H., Björkhem, I., Einarsson, C., 2002. Regulation of hepatic low-density
1100 lipoprotein receptor, 3-hydroxy-3-methylglutaryl coenzyme A reductase,
1101 and cholesterol 7 α -hydroxylase mRNAs in human liver. *The Journal of*
1102 *Clinical Endocrinology & Metabolism* 87 (9), 4307–4313.
- 1103 [31] Sanguinetti, G., Lawrence, N., Rattray, M., 2006. Probabilistic infer-
1104 ence of transcription factor concentrations and gene-specific regulatory
1105 activities. *Bioinformatics* 22 (22), 2775–2781.
- 1106 [32] Sebti, S., Hamilton, A., 1997. Inhibition of Ras prenylation: A novel ap-
1107 proach to cancer chemotherapy. *Pharmacology and Therapeutics* 74 (1),
1108 103–114.
- 1109 [33] Segal, I., 1975. *Enzyme kinetics behaviour and analysis of rapid equi-*
1110 *librium and steady-state enzyme systems*. A Wiley-Interscience Publi-
1111 cation, New York, USA.
- 1112 [34] Siperstein, M., Fagan, V., 1966. Feedback control of mevalonate syn-
1113 thesis by dietary cholesterol. *Journal of Biological Chemistry* 241 (3),
1114 602–609.
- 1115 [35] Srivastava, R., Ito, H., Hess, M., Srivastava, N., Schonfeld, G., 1995.
1116 Regulation of low density lipoprotein receptor gene expression in HepG2

- 1117 and Caco2 cells by palmitate, oleate, and 25-hydroxycholesterol. *Journal*
1118 *of lipid research* 36 (7), 1434–1446.
- 1119 [36] Tanaka, R., Edwards, P., Lan, S., Knöppel, E., Fogelman, A., 1982.
1120 Purification of 3-hydroxy-3-methylglutaryl coenzyme A reductase from
1121 human liver. *Journal of Lipid Research* 23 (4), 523–530.
- 1122 [37] Tansey, T., Shechter, I., 2000. Structure and regulation of mammalian
1123 squalene synthase. *Biochimica et Biophysica Acta-Molecular and Cell*
1124 *Biology of Lipids* 1529 (1), 49–62.
- 1125 [38] The Metabolomics Innovation Centre, Accessed: 31-07-2015. The
1126 human metabolome database. [http://www.hmdb.ca/metabolites/
1127 HMDB01375](http://www.hmdb.ca/metabolites/HMDB01375).
- 1128 [39] Trachsel, H., 1991. Translation in eukaryotes. CRC Press, Florida, USA.
- 1129 [40] Turley, S., Dietschy, J., 2003. The intestinal absorption of biliary and
1130 dietary cholesterol as a drug target for lowering the plasma cholesterol
1131 level. *Preventive Cardiology* 6 (1), 29–64.
- 1132 [41] Cards, G., Accessed: 15-10-2017. Hmgcr gene size. [http://www.
1133 genecards.org/cgi-bin/carddisp.pl?gene=HMGCRC](http://www.genecards.org/cgi-bin/carddisp.pl?gene=HMGCRC).
- 1134 [42] DNA technologies, I., Accessed: 17-10-2017. Molecular facts and figures.
1135 [https://www.idtdna.com/pages/docs/educational-resources/
1136 molecular-facts-and-figures.pdf?sfvrsn=4](https://www.idtdna.com/pages/docs/educational-resources/molecular-facts-and-figures.pdf?sfvrsn=4).
- 1137 [43] van Greevenbroek, M., de Bruin, T., 1998. Chylomicron synthesis by
1138 intestinal cells in vitro and in vivo. *Atherosclerosis* 141, S9–S16.
- 1139 [44] Vargas, N., Brewer, B., Rogers, T., Wilson, G., 2009. Protein kinase
1140 C activation stabilizes LDL receptor mRNA via the JNK pathway in
1141 HepG2 cells. *Journal of Lipid Research* 50 (3), 386–397.
- 1142 [45] Watterson, S., Guerriero, M., Blanc, M., Mazein, A., Loewe, L., Robert-
1143 son, K., Gibbs, H., Shui, G., Wenk, M., Hillston, J., P., G., 2013. A
1144 model of flux regulation in the cholesterol biosynthesis pathway: Im-
1145 mune mediated graduated flux reduction versus statin-like led stepped
1146 flux reduction. *Biochimie* 95 (3), 613–21.

- 1147 [46] Wilson, G., Deeley, R., 1995. An episomal expression vector system for
1148 monitoring sequence-specific effects on mRNA stability in human cell
1149 lines. *Plasmid* 33 (3), 198–207.
- 1150 [47] Yang, W., Swartz, J., 2011. A filter microplate assay for quantitative
1151 analysis of DNA binding proteins using fluorescent DNA. *Analytical*
1152 *Biochemistry* 415 (2), 168–174.